On the Sensitivity of Tropical Cyclone Intensification under Upper-Level Trough Forcing

Marie-Dominique Leroux, Matthieu Plu, Frank Roux

On the Sensitivity of Tropical Cyclone Intensification under Upper-Level Trough Forcing

MARIE-DOMINIQUE LEROUX

Laboratoire de l'Atmosphère et des Cyclones, Unité mixte 8105, CNRS/Météo-France/Université de La Réunion, Sainte Clotilde, La Réunion, France

MATTHIEU PLU

CNRM-GAME, Météo-France/CNRS, Toulouse, France

FRANK ROUX

Laboratoire d'Aérologie, UMR 5560, Université de Toulouse/CNRS, Toulouse, France

(Manuscript received 11 June 2015, in final form 7 December 2015)

ABSTRACT

This study is part of the efforts undertaken to resolve the ''bad trough/good trough'' issue for tropical cyclone (TC) intensity changes and to improve the prediction of these challenging events. Sensitivity experiments are run at 8-km resolution with vortex bogusing to extend the previous analysis of a real case of TC–trough interaction (Dora in 2007). The initial position and intensity of the TC are modified, leaving the trough unchanged to describe a realistic environment. Simulations are designed to analyze the sensitivity of TC prediction to both the variety of TC–trough configurations and the current uncertainty in model analysis of TC intensity and position.

Results show that TC intensification under upper-level forcing is greater for stronger vortices. The timing and geometry of the interaction between the two cyclonic potential vorticity anomalies associated with the cutoff low and the TC also play a major role in storm intensification. The intensification rate increases when the TC (initially located 12° northwest of the trough) is displaced 1° closer. By allowing a gradual deformation and equatorward tilting of the trough, both scenarios foster an extended ''inflow channel'' of cyclonic vorticity at midlevels toward the vortex inner core. Conversely, unfavorable interaction is found for vortices displaced 3° or 4° east or northeast. Variations in environmental forcing relative to the reference simulation illustrate that the relationship between intensity change and the 850–200-hPa wind shear is not systematic and that the 200-hPa divergence, 335–350-K mean potential vorticity, or 200-hPa relative eddy momentum fluxes may be better predictors of TC intensification during TC–trough interactions.

1. Introduction

The difficulty to accurately predict tropical cyclone (TC) intensification using numerical weather prediction models persists (WMO 2015), causing improvements in 24–72-h intensity forecasts to lag behind their counterpart track forecasts (DeMaria et al. 2014). It is, therefore, necessary to (i) quantify and communicate forecast uncertainty and (ii) unravel the mechanisms leading to TC spinup, and/or better resolve multiscale processes in prediction models. Indeed, both large-scale (e.g., Molinari and Vollaro 1989; Hanley et al. 2001; Davidson et al. 2008; Hendricks et al. 2010) and vortex-scale (e.g., Willoughby et al. 1982; Montgomery and Kallenbach 1997; Schubert et al. 1999; Wang 2002; Montgomery et al. 2006; Nguyen et al. 2011) processes have been demonstrated to control TC intensification.

Although the focus of the research community is mostly toward the dynamics of the storm's inner core within ~200 km of the storm center, the review presented at the Eighth WMO International Workshop on Tropical Cyclones (IWTC-8; Leroux et al. 2014) indicates that continued study of external influences on

Corresponding author address: Marie-Dominique Leroux, Cellule Recherche Cyclones, Météo-France DIROI, 50 Boulevard du Chaudron, 97491 Sainte Clotilde CEDEX, La Réunion, France.
E-mail: marie-dominique.leroux@meteo.fr

DOI: 10.1175/MWR-D-15-0224.1

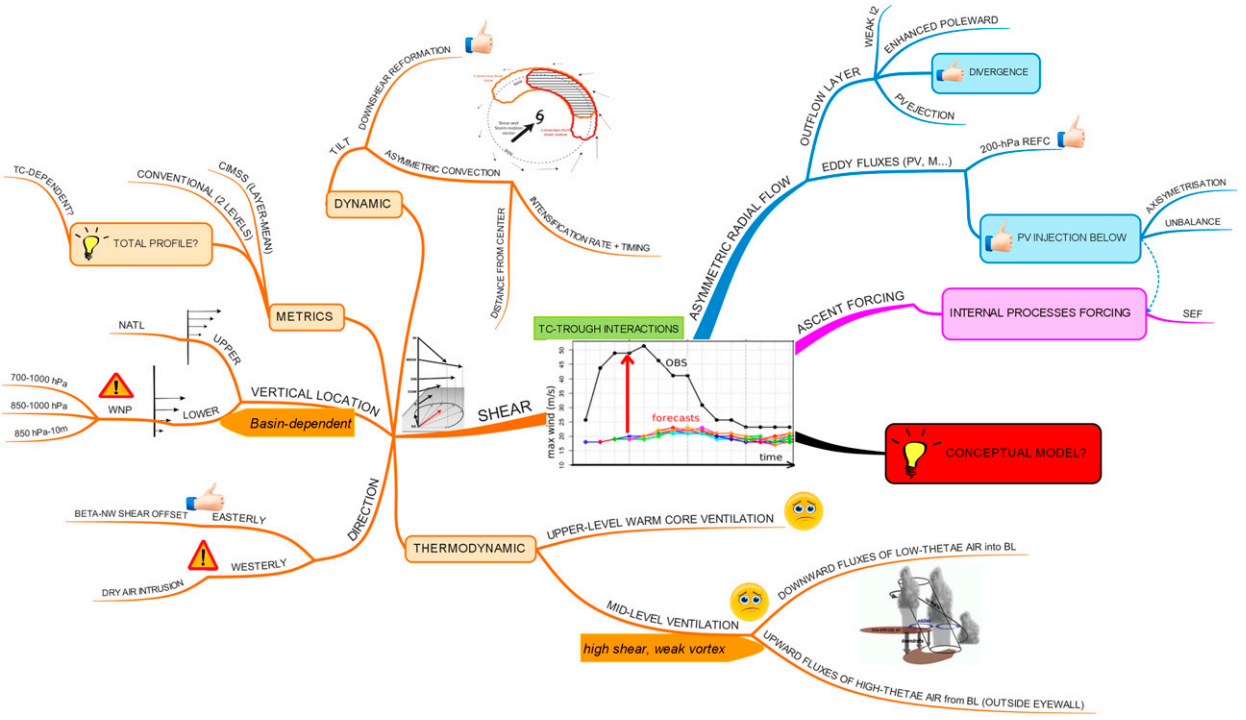

FIG. 1. Comprehensive map for studying the problem of TC intensity change under upper-level trough forcing. The BL stands for boundary layer, I2 for inertial stability, M for angular momentum, NATL for North Atlantic, NW for northwesterly, PV for potential vorticity, REFC for relative eddy momentum flux convergence, SEF for secondary eyewall formation, TC for tropical cyclone, and WNP for western North Pacific.

TC intensity change is warranted because the environment hostility controls both the development and predictability of TCs (Zhang and Tao 2013; Tao and Zhang 2014). The knowledge gaps or suitable research routes regarding the problem of TC intensity change under external influences are summarized in a comprehensive sketch (Leroux et al. 2014, see their Fig. 9).

Because it affects multiple environmental parameters, upper-level trough forcing, in particular, remains one of the strongest challenges of operational forecasting, as already recognized by the IWTC-6 (WMO 2007). Upper-level troughs or cutoff lows that interact with tropical cyclones usually result from the breaking of a planetary Rossby wave train originating from the midlatitudes that propagates equatorward into the subtropical latitudes. Such events are associated with an Ertel potential vorticity (PV) coherent structure at upper levels (Plu et al. 2008), also frequently referred to as a cyclonic (negative in the Southern Hemisphere) PV anomaly (Hoskins et al. 1985). An interaction is generally said to occur when the relative eddy momentum flux convergence (REFC; Molinari and Vollaro 1989) calculated at 200 hPa in a given annulus around the TC center, such as 300–600 km, exceeds $10\,\mathrm{m\,s^{-1}\,day^{-1}}$ for at least two consecutive 12-hourly time periods (DeMaria et al. 1993; Hanley et al. 2001). This parameter acts as a measure of the outflow layer spinup of the TC as a trough comes into the aforementioned annulus.

Upper-level troughs can alter the environment of TCs and may have different impacts on storm intensity (Fig. 1). The most documented perturbations are the following: significant vertical wind shear (usually detrimental; Kaplan and DeMaria 2003); increased upper-level divergence and enhanced outflow poleward of the storm (beneficial; Ritchie and Elsberry 2007); cyclonic eddy angular momentum import at upper levels (beneficial; Molinari et al. 1995); as well as cyclonic potential vorticity advection toward the TC core (Molinari et al. 1995, 1998; Bosart et al. 2000), which is beneficial below the level of the outflow anticyclone (''PV superposition principle''; Molinari et al. 1998).

In addition, an upper-level trough is associated with strong upper-level winds located on the polar side of any nearby TC. The so-called jet stream (Hoskins et al. 1985) may trigger vertical motion and convection by strong upper-level divergence in the jet entrance and exit regions. From mass-conservation arguments, this can lead to enhanced convergent inflow into the tropical cyclone. Dry-air intrusion from the lower stratosphere or the triggering of convection by upward velocities associated

with PV anomalies (Hoskins et al. 1985) in the vicinity of the inner core are other interesting processes that might play a role in TC–trough interactions. Leroux et al. (2013, hereafter L13), demonstrated that external forcing can also trigger secondary eyewall formation (SEF) and allow further storm intensification (Fig. 1). The authors explained how an upper-level trough can induce cyclonic spinup over the whole troposphere at outer radii.

Upper-level strong winds accompanying the main trough eastward translation generally modify the wind shear profile of the environment, both in magnitude and direction. Vertical wind shear (VWS) is known as one of the major synoptic-scale factors influencing TC intensity and its role has been carefully investigated (Fig. 1). Shear-induced ventilation can weaken a TC through three concomitant processes: (i) a dilution of the upper-level warm core by outward fluxes of high θ_e and PV values, which causes the central pressure to rise through hydrostatic arguments (Frank and Ritchie 2001; Zhang and Chen 2012); (ii) convective downdrafts that flush low-entropy air into the boundary layer (Riemer et al. 2010, 2013); and (iii) shear-induced updrafts outside the eyewall that transport high-entropy air from the boundary layer, further weakening the midlevel radial gradient of moist entropy across the eyewall (Gu et al. 2015). The importance of shear height on TC intensification is examined (Tang and Emanuel 2012; Shu et al. 2013; Wang et al. 2015) to possibly develop new metrics from the total vertical wind profile (Fig. 1). The shear also influences the spatial distribution of convection (Tao and Zhang 2014), inducing wavenumber-1 asymmetries with convection concentrated in the downshear-left quadrant for TCs in the Northern Hemisphere (Frank and Ritchie 2001; see our Fig. 1). By leading to increasingly asymmetric convection, azimuthally averaged heating at a larger radius, and thus slower storm development following the theories of Nolan et al. (2007) and Vigh and Schubert (2009), the shear can significantly affect the timing and rate of TC intensification. Finally, the direction of shear was also found to play a role in TC intensity change (Fig. 1). Overall, easterly shear, especially in the low to middle troposphere, has considerably weaker effects than westerly shear because part of the easterly shear could be offset by the beta-induced northwesterly shear (Zeng et al. 2010). Furthermore, westerly shear appears to promote the intrusion of dry environmental air in weakening TCs over the western North Pacific (Shu et al. 2014). In the idealized experiments of Ge et al. (2013), the relative location of dry air to the right of the VWS direction (in the Northern Hemisphere) appears especially detrimental to TC development because this dry air is subsequently advected by the vortex primary circulation to the downshear side and injected into the updrafts.

Although various mechanisms have been identified, no unified theory or conceptual model for the prediction of TC intensity under upper-level forcing has been developed. Such a guidance tool could provide forecasters with specific criteria to use, or suitable signatures to follow, in the various fields produced by a numerical weather prediction system. Currently being tested, a first conceptual model for the interaction of a TC with a tropical upper-tropospheric trough (TUTT) cell has been developed in the western North Pacific (Patla et al. 2009), but it is only designed for operational track guidance. Besides, such a model may not be suitable for interactions over other basins, and between TCs and troughs of midlatitude origin.

It is, therefore, not surprising that forecasters widely feel unequipped to deal with situations when some factors may favor development (or intensification) and others may oppose it. In particular, it is not known how quickly a TC may intensify or weaken as it interacts with troughs of various magnitudes and storm-relative positions. The problem can be illustrated with two cases observed in the southwest Indian Ocean: TC Dora on 31 January 2007 and TC Fobane on 7 February 2014 (Fig. 2). The storms likely had similar initial intensities, although their real intensities remain unclear because of (i) the uncertainty in TC intensity estimation over oceanic regions (in the best-track data, Dora is stronger than Fobane), (ii) initial model analysis error, and (iii) the resolution change in European Centre for Medium-Range Weather Forecasts (ECMWF) analyses from 2007 to 2014 that makes Fobane look stronger than Dora in the 850-hPa geopotential contours (Figs. 2a,b). But more interesting is the fact that the troughs, located some 1500 km southeast of the vortex centers and associated with strong cyclonic PV anomalies aloft (Figs. 2a, b), the storm tracks (not shown), and the ocean heat contents (not shown) had similar initial characteristics. However, despite such a similar TC–trough configuration, two very different scenarios of TC intensification occurred. Shortly after Dora entered the region with enhanced vertical shear, significant convergence replaced the divergence upshear and the divergence increased downshear in the middle to upper troposphere (Figs. 2a,c). Dora merged rapidly with the strong cyclonic vorticity injected from the 330-K (or 500 hPa) midlevel cutoff low that detached ahead of the trough while the main trough at 200 hPa stayed away (Figs. 2c,e, blue contours). In the course of 24 h, from t_1 + 12 to t_1 + 36 h, Dora deepened by 25 hPa. On the other hand, Fobane only deepened by 20 hPa during the 48-h period separating Figs. 2b and 2d and subsequently filled. At 200 hPa, the two vortices associated with the cutoff low and the storm rapidly rotated cyclonically around each other in

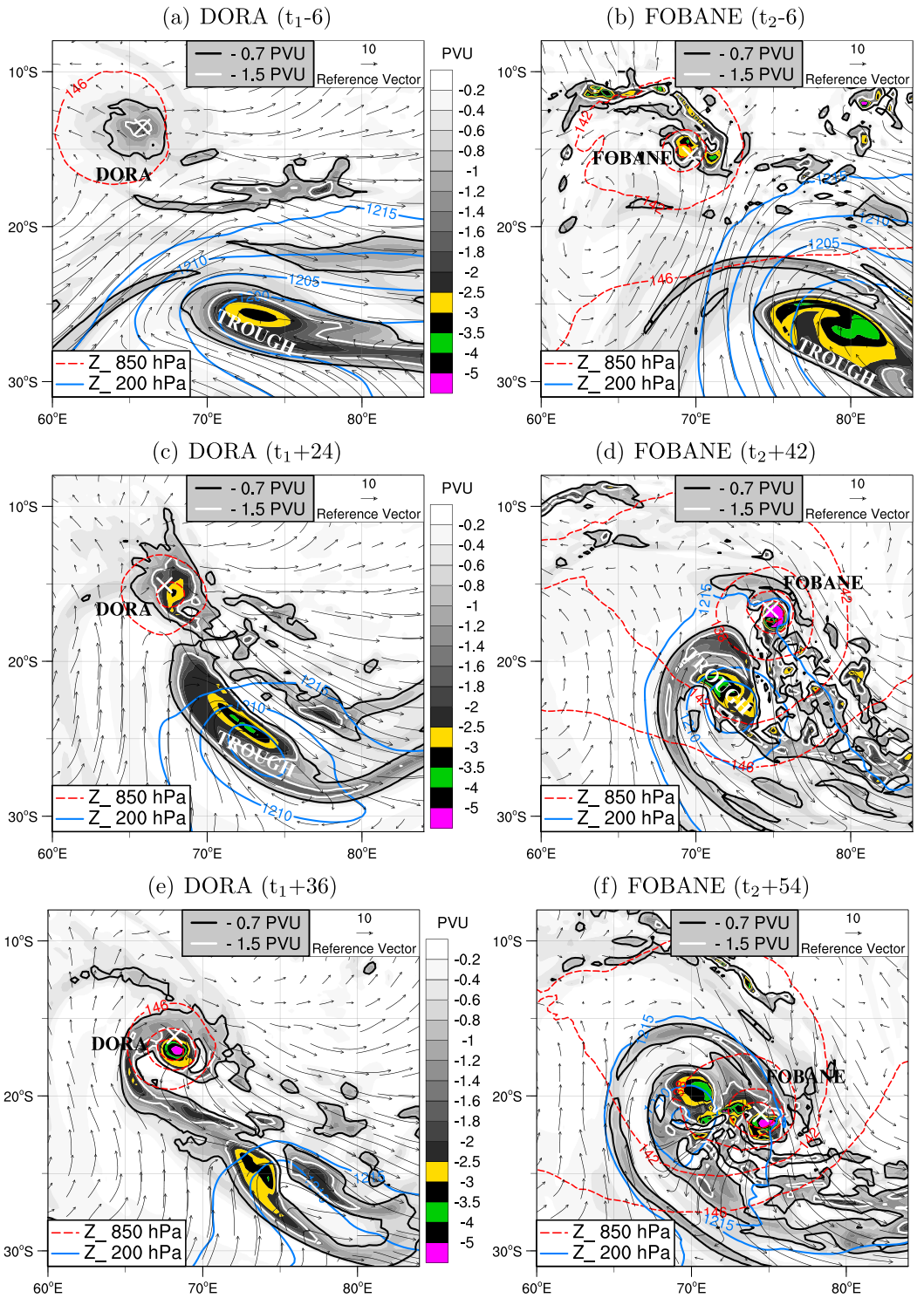

FIG. 2. ECMWF operational analyses for (left) TC Dora (a) 6 h before, (c) 24 h after, and (e) 36 h after t_1 = 0600 UTC 31 Jan 2007 vs (right) TC Fobane (b) 6 h before, (d) 42 h after, and (f) 54 h after t_2 = 1800 UTC 7 Feb 2014. Plotted are the 200-hPa wind vectors ($m\,s^{-1}$) and the 330-K Ertel potential vorticity field (1 PVU = $10^{-6}\,K\,kg^{-1}\,m^2\,s^{-1}$; negative, shaded with −0.7- and −1.5-PVU contours). Dashed red (solid blue) contours are geopotential height Z (gpm) at 850 (200) hPa and delineate the cyclonic circulations associated with the TC (the trough). A white × indicates the TC's best-track center. Horizontal model wavenumber varies from T799 in 2007 to T1279 in 2014, which corresponds to a grid spacing decreasing from 25 to 16 km.

accordance with a Fujiwhara (1921) effect before the 200-hPa low (Fig. 2f, blue contours) eventually moved on top of the TC circulation after 72 h, leading to Fobane's filling. In the meantime, midlevel (330 K) PV from the trough filamented and spiraled around the TC to eventually reach the vortex inner core (Fig. 2f).

To help forecasters tackle the "bad trough/good trough" (Hanley et al. 2001) issue, further investigation is, therefore, needed to understand and accurately predict the probable impact of an upper-level trough on TC intensity. Focused on a difficult forecast case, the present modeling study aims at evaluating the subtle variations in environmental forcing that can control the pace and nature of intensity change during TC–trough interactions. The methodology is new and differs from former numerical modeling studies that documented TC–trough interaction and its sensitivity. Previous research focused on the relative importance of trough strength and depth on TC intensification in an idealized framework (Kimball and Evans 2002) or used piecewise PV inversion to modify the characteristics of an upper-level low approaching a real hurricane (Shapiro and Möller 2003, 2005). Shieh et al. (2013) insisted on the importance of correctly capturing the structure of an upper-tropospheric trough and the associated diffluence–divergence magnitude, especially as the interaction alters both the trough, and TC structure and intensity. An important missing ingredient in these studies is the role of the TC vortex characteristics in the interaction. The sensitivity of TC–trough interaction to the initial TC position has been investigated in some detail in the context of extratropical transition by identifying bifurcation points in the steering flow (Riemer and Jones 2014; Pantillon et al. 2016). In this article, a real case of TC–trough interaction (Dora on 31 January 2007; L13) is used to run sensitivity experiments in which both the initial position and intensity of the TC are modified, leaving the trough unchanged. Relevant questions include: How much does model uncertainty in TC intensity and position analysis influence the reliability of TC–trough interaction prediction? How much does a weaker storm intensify under upper-level forcing compared to a stronger storm? Are the initial relative positions of a trough and a TC important in favoring good versus bad trough interaction? What is the dynamic impact of an external mid- to upper-level PV anomaly in vortex intensification? Which interactions with mid- to upper-tropospheric systems will lead to vortex intensification?

The present work begins in section 2 by quantifying the uncertainty in model analyses of TC intensity and position over the southwest Indian Ocean. Section 3 describes the case study and experimental setup. Section 4 analyses the impact of the initial geometry of the interaction on subsequent TC intensification and track. Section 5 further investigates particular simulations of interest. Section 6 gives a summary, presents the limitations of this study, and outlines possible future investigations.

2. TC analysis uncertainty over the southwest Indian Ocean

To quantify the uncertainty in model analyses of TC central pressure and position, basic statistics are conducted over the southwest Indian Ocean, the area of responsibility of the Regional Specialized Meteorological Center (RSMC), La Réunion, France, for tropical cyclone warnings. Five operational deterministic models are examined during 10 consecutive TC seasons since 2004. The predicted intensity and position of each system are compared to the corresponding best-track (BT) values at various lead times. The intensity of TCs is given in terms of the estimated minimum sea level pressure. The central pressure error (CPE) is defined as the absolute difference between the BT and forecast pressure minima. The direct position error (DPE) corresponds to the distance between the BT and forecast positions. Considering the very limited observations in the Indian Ocean, the BT estimates may not be as accurate as in other basins with aircraft reconnaissance. At times, especially far from land, the BT data consist of subjective Dvorak (1984) estimates. At other times, a variety of platforms including scatterometers, Advanced Microwave Sounding Unit (AMSU) intensity estimates, in situ surface observations, and land-based radars are available for use in intensity and structural analysis of the cyclone.

Global models include those from the Met Office (UKMO), the Integrated Forecast System (IFS) developed by the ECMWF, and Météo-France's Action de Recherche Petite Echelle Grande Echelle (ARPEGE) developed in parallel with IFS (Yessad 2015). Two limited-area models designed for the prediction of tropical cyclones that both use vortex bogusing (TC vortex replacement or assimilation of synthetic TC data alongside conventional observations) are also evaluated: the Geophysical Fluid Dynamics Laboratory (GFDL) Navy model (GFDN) and Météo-France's regional version of the ARPEGE model (ALADIN-Réunion) that became operational in the southwest Indian Ocean in 2006. Details of each model's configuration can be found in Heming and Goerss (2010). Even though statistics are based on a homogeneous sample of tropical systems, run times vary among models; the total number of forecasts processed per model is indicated in Table 1.

TABLE 1. Overall performance of five operational models at 0-, 24-, 48-, and 72-h lead times in the southwest Indian Ocean during 10 TC seasons (2004–05 to 2013–14): central pressure mean (CPE) and root-mean-square (CP-RMSE) errors (hPa), as well as direct position mean (DPE) and root-mean-square (DP-RMSE) errors for corresponding positions (km). Note that only eight seasons were used to compute the Aladin-Réunion statistics since the model only became operational in 2006. The *N* indicates the sample size.

	ECMWF				UKMO				ARPEGE				GFDN				Aladin			
Forecast time (h)	0	24	48	72	0	24	48	72	0	24	48	72	0	24	48	72	0	24	48	72
CPE (hPa)	10	11	11	10	12	13	13	13	13	13	13	12	6	11	13	14	8	10	12	11
CP-RMSE (hPa)	14	15	16	16	14	15	15	15	16	16	16	16	15	20	23	26	12	14	16	15
N	1571	1175	1053	913	1176	1057	929	723	1277	1122	991	842	1746	1642	1507	1299	917	819	598	405
DPE (km)	73	110	170	243	55	150	261	398	94	173	277	384	38	153	272	385	68	142	233	350
DP-RMSE (km)	69	85	109	161	49	91	153	254	74	121	183	586	38	94	161	221	72	106	148	236
N	1601	1235	1123	976	1203	111	987	773	1304	1178	1049	897	1794	1734	1612	1400	940	858	632	438

Statistics from these five models (Table 1) suggest that the mean absolute error for TC central pressure at the initial time of the forecast is about 10 hPa on average since 2004, with a slight decrease with time (not shown), and the standard deviation is about 14 hPa. Results also indicate that the average initial position error is about 70 km for the five models with a 60-km mean standard deviation. As expected, the downward time trend is larger for the mean position error than for intensity (not shown). At short term (0–24 h), the best results in intensity and position forecasts are from the two limited-area models owing to vortex bogusing. This is consistent with recent statistics obtained over the Australian region using a sample of 22 forecasts of two major TCs (see Table 4 of Davidson et al. 2014): the Australian Community Climate and Earth System Simulator (ACCESS-A; Puri et al. 2013) showed an average mean absolute error of 11 hPa and 117 km at the initial time of the forecast, while the average error was reduced to 7 hPa and 30 km in the version of the model that uses vortex bogusing (ACCESS-TC; Davidson et al. 2014). However, at longer ranges (48–72 h), ECMWF performs better thanks to a more coherent representation of the interaction between the storms and their large-scale environments. The initial position and intensity errors obtained in this section will be used as benchmarks for changing the vortex initialization in our experiments (section 3c).

Table 1 also shows that CPE has little dependence on lead time for the three global models. This is different from the more common error growth computed from statistics of official RSMCs forecasts, because forecasters gather information from various sources (statistic, deterministic, ensemble, and/or consensus forecasts). Aemisegger (2009) also found a non-significant concave form of the CPE curve after about 60-h lead time when looking at ECMWF operational TC forecasts over the 2005–08 period. The reason for this trend is unclear but we note that the initial CPE error in large-scale models is large, probably due to their coarse-resolution analysis with a storm's eye of the size of the model resolution. On the contrary, higher-resolution models with vortex specification, such as Aladin-Réunion and GFDN, benefit from a reduced initial pressure error but error growth makes them less competitive after midterm ranges.

3. Case study and experimental setup

a. TC Dora

Tropical Cyclone Dora (2007) deepened in the southwest Indian Ocean under hardly conducive conditions: moderate-to-strong ambient 850–200-hPa wind shear (above 9 m s^{-1} during 36 h, peaking at 12 m s^{-1}), and ocean heat content below the 50 kJ cm^{-2} threshold that has been shown to promote high rates of intensity change (Shay et al. 2000). Rapid intensification[1] occurred between 1800 UTC 31 January and 0000 UTC 3 February with a 50-hPa pressure fall from 975 hPa (see Fig. 1 of L13). The intensification was temporarily slowed down by an eyewall replacement cycle (ERC; Willoughby et al. 1982) from late 1 February to early 2 February.

Dora was approached by an upper-level trough associated with a planetary Rossby wave train originating from the midlatitudes. A strong negative (cyclonic) PV anomaly associated with a cutoff cyclone formed during the isentropic equatorward advection of stratospheric air into the troposphere. This PV anomaly was located about 12° southeast of Dora's center on 0600 UTC 31 January 2007, 12 h before the onset of RI (Fig. 3). This is within the 15° effective interaction radius used by Patla et al. (2009) in their conceptual model of TC–TUTT cell interaction for TC motion.

[1] Rapid intensification (RI) is defined in the North Atlantic by an increase of the maximum sustained surface winds above 30 kt (15.4 m s^{-1}) in the course of 24 h (Kaplan and DeMaria 2003). We use the same threshold for tropical cyclones in the southwest Indian Ocean.

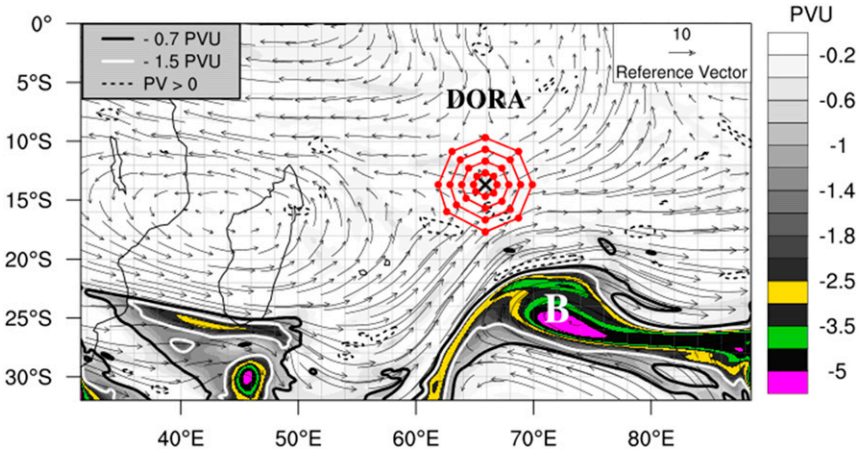

FIG. 3. Wind vectors (arrows, m s^{-1}) and PV (PVU; negative, shaded with −0.7- and −1.5-PVU contours; positive, 0.2-PVU dotted contours) at 200 hPa at the initial time t_0 of the reference simulation (0600 UTC 31 Jan 2007). A black × indicates Dora's BT center. Red dots delineate the various initial vortex positions in the sensitivity experiments. Label B indicates the coherent structure (cutoff low) approaching TC Dora.

b. *The reference experiment*

A control run (hereafter called reference experiment) of TC Dora was previously examined by L13. It provided reliable information on the track and the vortex response to the external forcing as it captured many observed characteristics of the storm and key aspects of the interaction, such as the tongue of dry air that gradually encircled the western side of TC Dora in association with the stratospheric intrusion. This 60-h forecast, initialized at t_0 = 0600 UTC 31 January, was carried out using the limited-area atmospheric model Aladin-Réunion (Montroty et al. 2008) in its 2011 operational configuration (hydrostatic, 70 vertical levels, 8-km horizontal resolution, and a fixed domain shown in Fig. 3). Earlier initial times were tried out but the model was less skillful in predicting the evolution of storm intensity. The initial and lateral boundary conditions were provided by ECMWF global analyses.

To obtain a realistic vortex structure and position at the base time of the forecast, the Aladin's three-dimensional variational data assimilation (3D-Var) of cyclone wind bogus (Montroty et al. 2008) was employed. Synthetic wind observations deduced from the Holland (1980) analytical model, plus the mean sea level pressure at the TC center, were produced from the surface to 500 hPa. Winds were derived at four radii (30, 50, 100, and 200 km) in order to force a realistic representation of the inner-storm structure. These pseudo-observations were assimilated at 0600 UTC 31 January 2007 in an Aladin's first-guess 6-h forecast initialized with an interpolation of the 25-km resolution IFS analysis at 0000 UTC 31 January 2007. One of the advantages of the Aladin-Réunion cyclone initialization is that the 3D-Var introduces realistic balance between the thermodynamic and dynamic fields (wind, temperature, humidity) and thus helps to equilibrate the vortex in the analyses and in the very first forecast hours (Montroty et al. 2008).

In the reference simulation, deviations in initial TC position and intensity from the BT were 5 km and 17.1 hPa, respectively, that is slightly below (above) the average position (intensity) uncertainties in operational analyses (section 2). Prediction of track was successful with errors less than 100 km during the 60-h forecast, which is quite competitive by international standards (Franklin 2008). But more importantly, the model captured the PV interaction as well as the two periods of RI (see Fig. 4 of L13). Aladin-Réunion was, thus, believed to provide reliable information on the response of the vortex to the external forcing. The main mechanisms identified for vortex intensification were PV advection toward the TC core between about 33 and 40 h, followed by secondary eyewall formation induced by eddy angular momentum flux convergence, eddy PV fluxes, and vertical velocity forcing from the trough (L13).

c. *Sensitivity tests*

For the current study, an ensemble of 98 experiments was performed using the same initial time t_0 and numerical setup as in L13, but with different initial conditions. Using Aladin's vortex specification routine, the storm is moved 1°, 2°, 3°, or 4° away from the best-track position in eight different octants, as illustrated in Fig. 3 (red dots). Such values allow us to take into account the

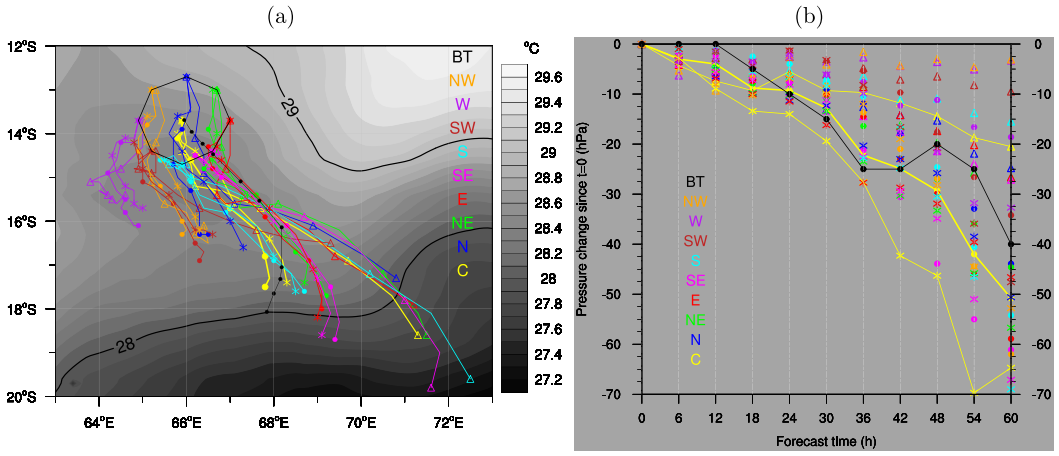

FIG. 4. (a) Tracks and (b) pressure change of the 24 vortices initially shifted 1° from the BT center in eight different octants. Colors indicate the quadrant (NW to N) in which the initial vortex is displaced while different symbols show the vortex initial intensity: circles for a BT intensity and triangles (asterisks) for a lower (higher) intensity. The octagon in (a) joins the eight different initial vortex positions as in Fig. 3. The three vortices initialized at the BT position (C, in yellow) with different intensities are also displayed (the thick yellow line with circles corresponds to the reference experiment). The best track is shown in black for comparison. The sea surface temperature field (°C) is shown with both black contours and black to white shading in (a).

variety of observed TC–trough interactions as well as the uncertainty in the analyzed TC and trough positions (via their relative distance). With a maximum 4° shift of the TC vortex, the initial separation distance between the two lows varies from 8° to 16° in our experiments. For comparison, Kimball and Evans (2002) placed the PV maximum 800 km west of the vortex center in their idealized experiments. Likewise, the PV coherent structure used to evaluate the contribution of the trough to Opal's intensification (Shapiro and Möller 2003) was located outside the 467-km radius in the northern sector of the storm.

Also, considering a mean 10-hPa error in TC initial intensity from model analyses (section 2) or from observations, three values were tested for initial vortex central pressure (CP_0): 975 (the BT value used in the reference experiment), 990, and 960 hPa. These values were chosen because they were observed or estimated at other times of the storm's life cycle, which allowed us to constrain the bogused vortex with consistent values of the radius of maximum winds (RMW) obtained from the BT dataset. The best track includes wind measurements from two Aeroclippers, or low-level balloon-borne instrumented platforms (Duvel et al. 2009), that were able to measure Dora's inner eyewall maximum wind speed and its location from 29 January to 6 February. After the assimilation process, the retained central pressures for the weak (strong) vortices are about 10 hPa above (below) that of the reference experiment at the initial time, which is within the range of intensity analysis error.

The original vortex from the ECMWF analysis is located some 180 km west-southwest of Dora's BT center at the initial time of the forecast t_0. Vortex filtering is not used in Aladin-Réunion. The reason is twofold: (i) the initial ECMWF analyzed vortex is very weak (1006 hPa at the surface center here) and (ii) any method used to extract vortices from model analyses has its limitations and can perturb the native environment of the storm. In this study, a very weak, isolated, ECMWF vortex can be spotted at 850 hPa in the initial wind field for some sensitivity experiments, mostly those where the bogus vortex is implanted in the eastern octants at some distance from the BT center (at least 2° for weak vortices and 3° for others). It was ensured that the remnant ECMWF vortex (i) was shallow (i.e., not visible at 500 hPa), and (ii) disappeared within 24 h of the forecast while moving to the west, without interacting with the bogused vortex. Also, to stay in realistic conditions, all simulations are initialized with the same operational sea surface temperature (SST) field illustrated in Fig. 4a (black and white shading).

d. Diagnostics

The minimum sea level pressure (MSLP) at the storm center is used to diagnose TC intensity. It was ensured that results were robust when using a different intensity metric such as the maximum surface wind speed. To assess the influence of initial vortex position, key large-scale parameters that have been demonstrated to influence the intensity of TCs approached by a trough are computed every 6 h for each sensitivity experiment. When time averages are used, they are generally

TABLE 2. The 60-h central pressure change (hPa) relative to the reference experiment and to the initial time for 98 experiments. The pressure values 960, 975, and 990 hPa refer to the three pressure initializations (CP_0).

	Shift											
	1°			2°			3°			4°		
Octant	960	975	990	960	975	990	960	975	990	960	975	990
C		−13.9				0					30.3	
N	0.2	6.9	26	−4.1	23.9	42.3	10.9	0.7	36.8	15	34.4	45.2
NE	−5.9	6.2	24.1	−5.3	4.8	26.6	22.2	27.9	32.8	33	26.6	34
E	4.2	−8.1	24.2	3.1	13.6	35.1	32.8	31	39.3	37.4	32.5	41.5
SE	−16.3	−10.3	23.7	10.7	15.7	32.7	21.6	17.4	36.3	39.8	33.1	43.9
S	−18.2	−3.4	35.3	12.7	7.6	35.1	10.8	14.1	42.9	14.7	37.6	47
SW	3.2	16.6	41.3	38.1	35	50.6	38	31.5	46.5	37.4	33.5	47.8
W	18.1	32.2	47.5	28.6	30.4	49.2	44.3	47.7	50.1	47.5	44	52.1
NW	−2	−11.2	47.7	40.8	43.7	48.4	42.8	44.8	47.2	38.4	41.6	46.8

computed over a 12–60-h period to exclude any possible disturbance from the model initial adjustment. When not explicitly stated, parameters are averaged over a 200–800-km annulus surrounding the predicted storm center, which excludes the inner-core circulation (as in Kaplan and DeMaria 2003).

Kinematic parameters include the 850–200-hPa VWS and 200-hPa divergence (DIV). The PV is averaged over the 335–350-K layer (about 450–200 hPa) to take into account the vertical extension of the PV anomaly approaching Dora. In the reference experiment, the trough-induced flow forced cyclonic PV advection into the TC core within a deep tropospheric layer above 335 K (L13). Also of importance is the inward eddy flux of cyclonic momentum detected in the upper troposphere of intensifying storms (Pfeffer and Challa 1981). The REFC [see Eq. (2) in DeMaria and Kaplan (1994)] is calculated at 200 hPa. Spanning from 100 km for the inner radii to 800 km for the outer radii, several radial ranges were tested such as 300–600 km to follow L13, DeMaria et al. (1993), or Hanley et al. (2001).

Finally, to assess the ocean thermodynamic impact on TC intensity, and distinguish it from any trough effect, SSTs are averaged over a 200-km-radius disk, where SST is known to influence TC intensity (Cione and Uhlhorn 2003), with cyclone-induced cooling extending typically over five radii of maximum wind (Vincent et al. 2012). Chan et al. (2001) demonstrated, from a simple ocean–atmosphere coupled model, that the expected rate of change in TC intensity with respect to SST at 48 h is of the order of 16 hPa °C^{-1} for SSTs between 27° and 30°C. Regarding the impact of SST on maximum potential intensity, Holland (1997) suggested a 10.5 hPa °C^{-1} sensitivity between 20° and 31°C (see his Table 2), based on the Carnot engine concept of Emanuel (1991). However, using a thermodynamic approach, he found that the sensitivity may range between 20 and 35 hPa °C^{-1} for SSTs between 27° and 31°C.

4. Sensitivity of TC–trough interaction to vortex position and strength

This section first quantifies forecast uncertainty from current average errors in numerical weather prediction (NWP) analyses for a TC such as Dora. The influence of vortex initial intensity and position on TC intensity prediction is then analyzed in the context of TC–trough interaction. Finally, several environmental parameters and their variations relative to the reference simulation are examined statistically to identify fundamental relationships with TC intensity change.

a. Quantifying forecast uncertainty

For vortices placed at the BT position, the 60-h central pressure change relative to the reference experiment and to the initial time varies from +30 hPa for an initial 990-hPa value to −14 hPa for a 960-hPa initialization (Table 2), with a peak of −27.7 hPa at 54 h (Fig. 5, black stars). For an initial 1° shift of the vortex center in the eight different octants, the pressure difference varies from +23 to +48 hPa for a 990-hPa initialization, −11 to +32 hPa for a 975-hPa initialization with a peak of −14.6 hPa at 48 h (Fig. 5), and −18 to +18 hPa for a 960-hPa initialization (Table 2). These results show that a 1° error in initial vortex location or a 10-hPa error in initial vortex intensity can cause a large spread in the intensification predicted at 54 or 60 h, ranging from −28 to +48 hPa in the case of this TC–trough interaction event.

b. Sensitivity to vortex initial intensity

The evolution of the predicted pressure along the 60-h forecast indicates that a stronger initial vortex placed at the same initial location as Dora has a greater intensification rate after 36 h (Fig. 5, black stars). On the contrary, a weaker initial vortex intensifies less (Fig. 5, black triangles). With a track almost identical to that of the reference experiment, and, hence, insignificantly

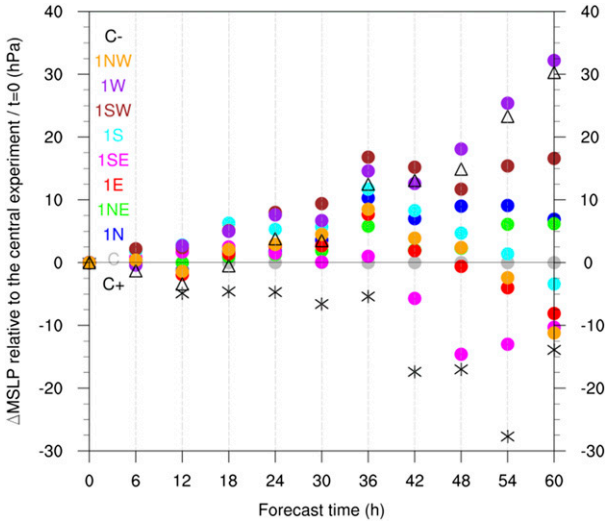

FIG. 5. Evolution of the predicted central pressure change relative to the reference experiment and to the initial time (ΔMSLP, hPa) for 10 experiments: 8 of them are initialized with the BT intensity at 1° distance from the BT center (circles; colors indicate the quadrant to which the initial vortex is displaced), the 2 others are initialized at the BT position with a higher (C+, black asterisks) or lower (C−, black triangles) intensity. The reference experiment is indicated in gray.

lower SSTs (−0.03°C on average over 200 km and 60 h), the intensification of the stronger vortex is most likely related to a favorable interaction between the TC and the trough in the 500–300-hPa layer. At 400 hPa for example—where the two PV anomalies associated with the trough and the TC have similar magnitudes—cyclonic PV advection from the trough into the TC core begins at 33 h, as in the reference experiment, but lasts longer (at least 12 more hours) thanks to enhanced confluence ahead of the trough (Figs. 6a–f). Vertical cross sections are plotted in the south-southwestern sector of the storm (azimuth 190°), where the midlevel inflow imposed by the trough is maximum near the storm center (Fig. 7). They indicate that the trough deforms and tilts toward the equator at midlevels, allowing direct advection of cyclonic PV values into the TC core within a 500–300-hPa layer. Radial PV advection (gray shading) into the TC center lasts longer for the stronger initial vortex compared to the reference experiment (Figs. 7a–f); PV anomalies delineated by the −0.7-PVU contour almost merge at 48 h (Fig. 7f). On the contrary, the interaction occurs later than in the reference experiment for a weaker initial vortex (not shown): radial inflow and PV advection reach the storm inner core at 48 h, possibly explaining the lower rate of intensification of the weaker initial vortex.

It can be concluded that such TC–trough configuration, with a deep trough initially located 12° southeast of the storm's center as originally observed for TC Dora, fosters the development of a mid- to upper-level "inflow channel." Results further demonstrate that this midlevel inflow channel (i) takes more time to reach the TC inner core when the vortex is initially weaker, and (ii) can be maintained for a longer period when the vortex is initially stronger. Potential vorticity advection and its effect on vortex intensity change will be further discussed in section 5.

Note that vertical cross sections of the relative humidity further indicate that the "PV inflow channel" is enclosed within a larger and thicker channel of dry air (not shown). On average the driest air is found in a 600–250-hPa layer in the 200–700-km radius range. It can also be seen that the inner cores of both a stronger initial BT-position vortex (C+) and a BT-intensity vortex initially displaced 1° southeast (1SE) are more resilient to that dry air. The role of the dry air will be further investigated in section 4c and in section 5. Other diagnostics were examined such as the pseudoadiabatic or the equivalent potential temperature (Bolton 1980), or the moist-air potential vorticity derived by using a specific entropy formulation expressed in terms of a moist-air entropy potential temperature (Marquet 2014). They did not provide a better conceptual view of that inflow channel.

The overall evolution of the predicted minimum surface pressure in the 99 experiments illustrates that the interaction with the trough promotes higher rates of intensification for initially stronger vortices (Table 2). The pressure change is considerably lower for depressions, as illustrated for an initial 1° shift of the vortex center (Fig. 4b, triangles). As a result, the weaker initial vortices (33 experiments) systematically deviate to the east (e.g., triangles in Fig. 4a). This is due to a smaller vertical extent of the vortex, which lowers the depth of the steering flow that influences the storm track. For a few experiments (especially those with a 3° or 4° initial shift), the storm goes very close to the eastern border of the domain where diagnostic variables can hardly be computed in a 200–800-km radial region centered on the storm. Therefore, the analysis will hereafter focus on the remaining 65 sensitivity experiments that have tracks analogous to that of the reference experiment with a general southward then southeastward motion, before veering to the south-southwest at the end of the forecast, as illustrated in Fig. 4a.

c. *Sensitivity to vortex initial position*

For simplicity, only the results from the 32 experiments initialized with the BT intensity (as in the reference experiment) are presented in this section. The other 33 experiments initialized with a stronger vortex give similar conclusions regarding the favored octants for TC intensification.

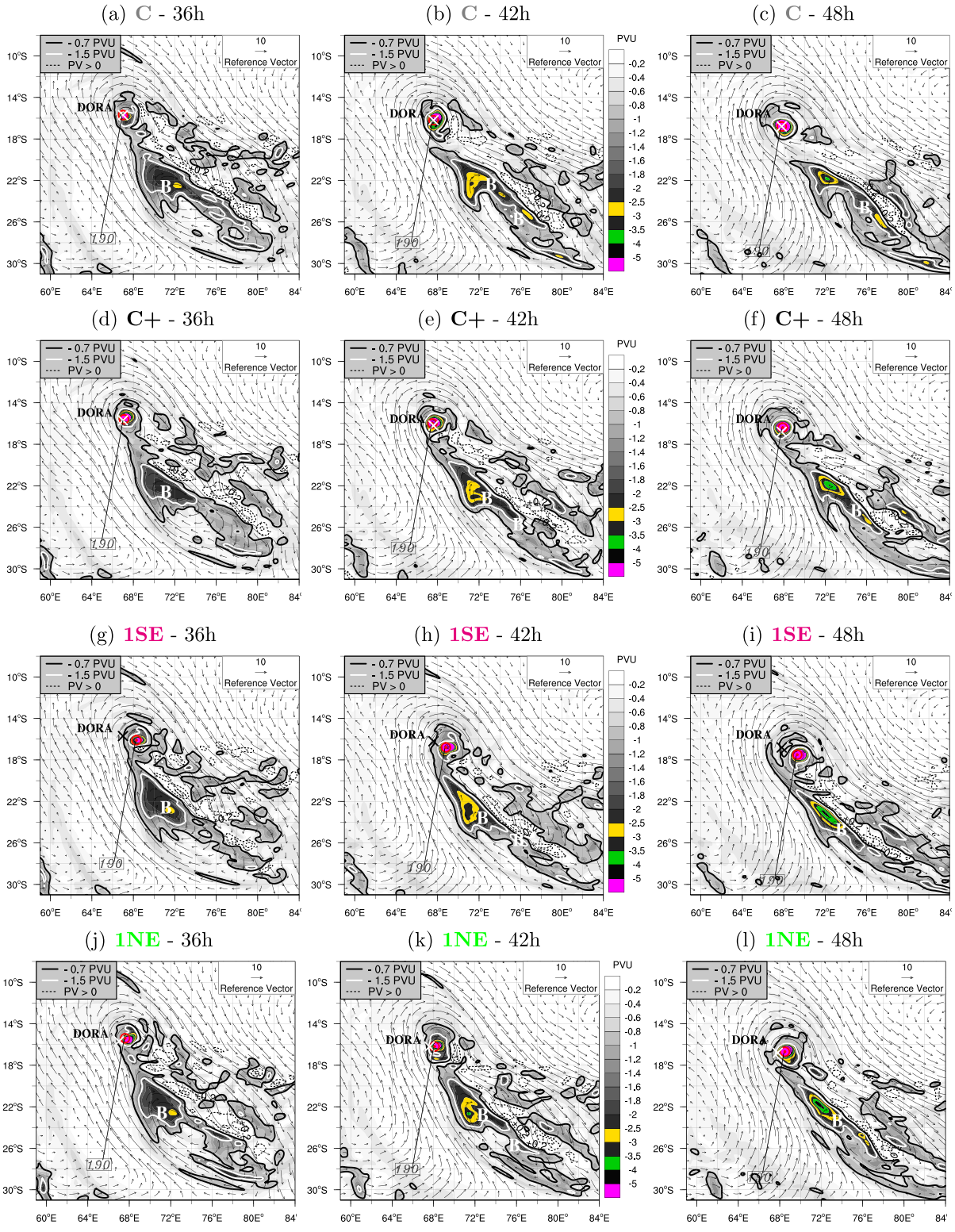

FIG. 6. As in Fig. 3, but at 400 hPa after (left to right) 36, 42, and 48 h of model integration from t_0 for (top to bottom) four experiments: the reference (C), a stronger initial BT-position vortex (C+), and a BT-intensity vortex initially displaced 1° southeast (1SE) and northeast (1NE). The red encircled dot (white or black cross) indicates the vortex predicted center in the simulation (in the reference experiment). A black straight line starting from the TC predicted center delineates the 1200-km-long cross section (azimuth 190°). Labels B indicate main PV advection from the coherent structure toward TC Dora.

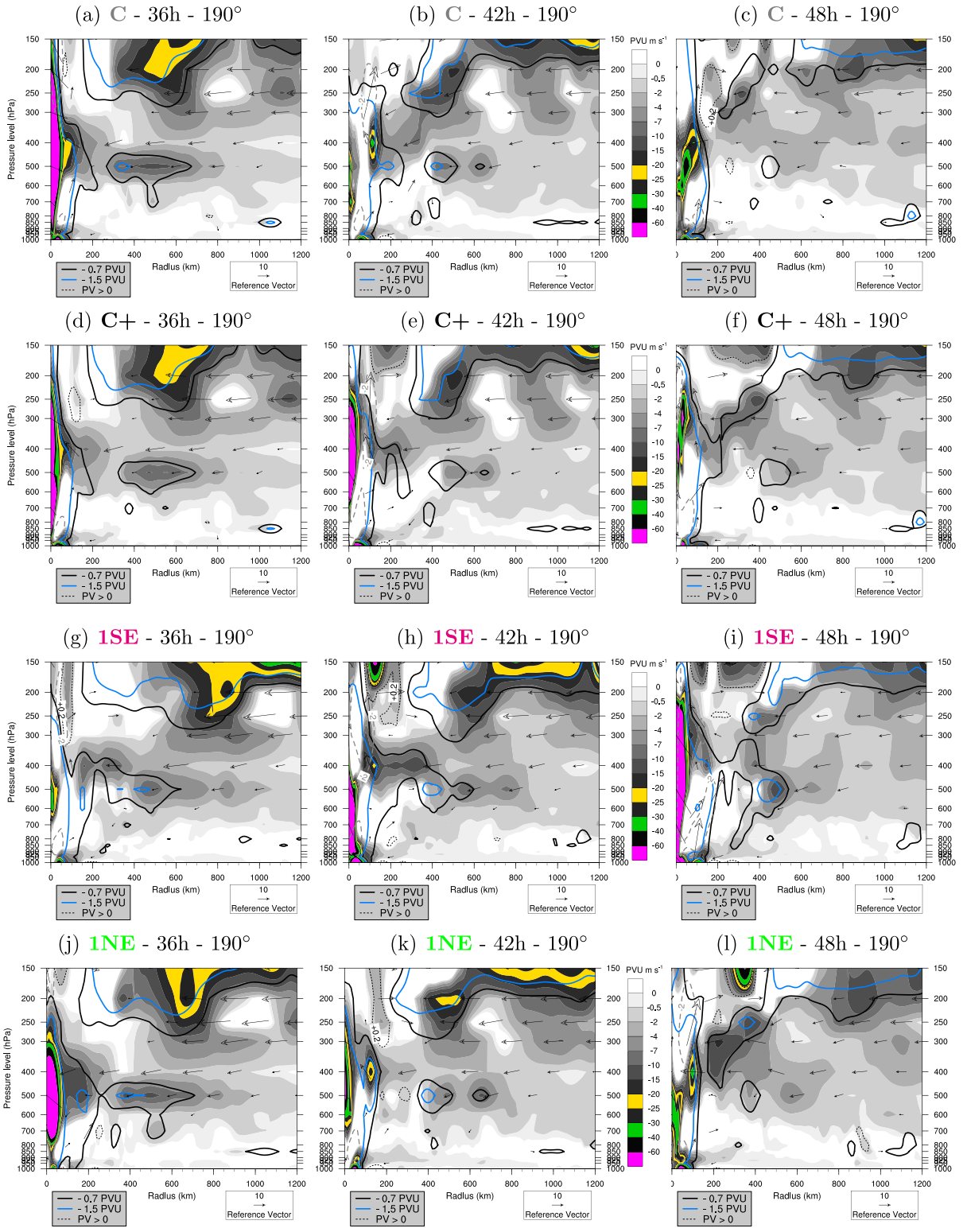

FIG. 7. As in Fig. 6, but for radius–pressure cross sections of negative values of PV radial advection $-u \times$ PV ($\mathrm{m\,s^{-1}} \times$ PVU, shaded) along a 190° azimuth (as delineated on horizontal maps in Fig. 6). Superimposed are PV contours of −0.7, −1.5, and 0.2 PVU. The TC center is located at the left. Arrows represent the radial and vertical wind vectors with vertical motion w ($\mathrm{m\,s^{-1}}$) approximated by $-\omega/10$. Dashed gray contours indicate regions of vertical velocity $<-2\,\mathrm{Pa\,s^{-1}}$.

Pressure forecasts indicate that for an initial distance larger than 1°, no vortex initialized at 975 hPa intensifies more than the reference experiment at t_0 + 60 h (Table 2), even when the displacement is toward the northeast where better conditions for SST and upper-level divergence are met (Fig. 8). This suggests that a favorable phasing of the TC and trough positions is needed for strong intensification to occur. In contrast, four of the eight vortices initially displaced by 1° get stronger than the reference experiment vortex at t_0 + 60 h, due to a greater intensification rate after 36 h (Fig. 5): the one shifted to the northwest (1NW), with the help of increased SSTs (Fig. 4a), and the three vortices that move over colder seas in the south, southeast, and eastern octants (1S, 1SE, and 1E). The vortex initialized in the southeastern quadrant in particular deepens by more than 10 hPa (−14.6 hPa at 48 h). Once again, this result seems correlated with a greater and longer (at least 24 more hours) PV advection at 400 hPa when the TC is closer to the cutoff low (Figs. 6g–i and 7g–i).

Figure 8 summarizes the influence of the four key parameters introduced in section 3d, averaged over the 12–60-h period for each of the 32 sensitivity forecasts. Each parameter is determined favorable or unfavorable by comparing its mean value with that in the reference experiment. SSTs are colder in the south, southeastern, and eastern octants (down to −0.35°C on average), which is consistent with the latitudinal gradient of SSTs (Fig. 8d). The storm's environment (in a 200–800-km annulus) becomes consistently more cyclonic (PV < 0) when the vortex is initially moved to the south, southeast, east, and to a lesser extent, northeast (Fig. 8c). Vortices displaced farther southeast, east, and northeast experience more divergence at 200 hPa (Fig. 8b), while the shear increases for all octants but in the south and north where it does not change much (Fig. 8a). The weak shear modification in the southern and northern octants results from the cumulative effect of successive periods of alternatively stronger or weaker shear (not shown). Results computed over a 12–36-h (not shown) or a 12–42-h period (Fig. 8, second row) show that the shear is more favorable, with up to 3 m s^{-1} decrease, for a southern vortex at earlier times of the forecast.

For all parameters, the favorable or unfavorable trend generally increases with initial distance from the BT center and changes are quasi linear for the mean PV (not shown). The 335–350-K PV parameter is, therefore, a good indication of the trough proximity. It is important to note that the shear and upper-level divergence, averaged over a 200–800-km annulus, do not systematically evolve in the same way. In three octants (southeast, east, and northeast), both the shear and the ambient divergence increase (Fig. 9). However, with a cutoff low originally located southeast of the storm, when the initial vortex is displaced to the southwest, west, or northwest, the shear intensifies and the divergence decreases compared to the reference experiment, setting a less favorable environment for storm intensification.

For a same shear intensity and storm movement, the wind shear direction may also contribute to differences in vortex intensification. While the reference vortex is southwesterly sheared over the 60-h period, vortices displaced to the north or to the three western octants experience an ambient south-southwesterly wind shear. The western vortices also experience drier environmental air from mid- to upper levels in association with the stratospheric air intrusion of the Rossby wave breaking event. The relative location of the dry air to the left of the VWS direction appears more detrimental to TC development (Fig. 5) because this dry air is subsequently advected by the vortex primary circulation to the downshear side and injected into the forced updrafts as in Ge et al. (2013). An illustration is given for the vortex displaced 1° west (Figs. 10b,d,f): dry subsident air beneath the trough progressively invades half of the inner core while strong upward motion at 500 hPa exists in the downshear quadrant and is dynamically enhanced ahead of the trough. The shear veers to west-southwesterly for vortices initiated in the southern and three eastern octants of the BT location, which seems more favorable for storm intensification considering the more important 60-h pressure drop predicted for three of these four vortices (Fig. 5). As anticipated, the eastern (western) quadrant is associated with extreme west-southwesterly (south-southwesterly) wind shear.

d. Statistical relationships between variables for 65 experiments

To characterize and quantify atmospheric environmental changes for various initial positions and intensities of the vortex, diagnostics from the 65-member sample are examined statistically. Differences with respect to the reference experiment are computed for every area-averaged parameter (previously defined in section 3d) with a 6-h time interval. The MSLP parameter is the pressure change computed from time t_0, as in Table 2. The signs of some parameters, such as PV and REFC, are reversed so that they become positive for cyclonic values, like in the Northern Hemisphere. Standard linear regression is used to determine relationships between variables. Statistical significance is verified for each sample size using the Student's t test at the 95% level. The information is displayed through scatterplots and cross correlations between diagnostic variables (Fig. 11). When the proportion of the variance in y explained by the variance in x exceeds 50%, the

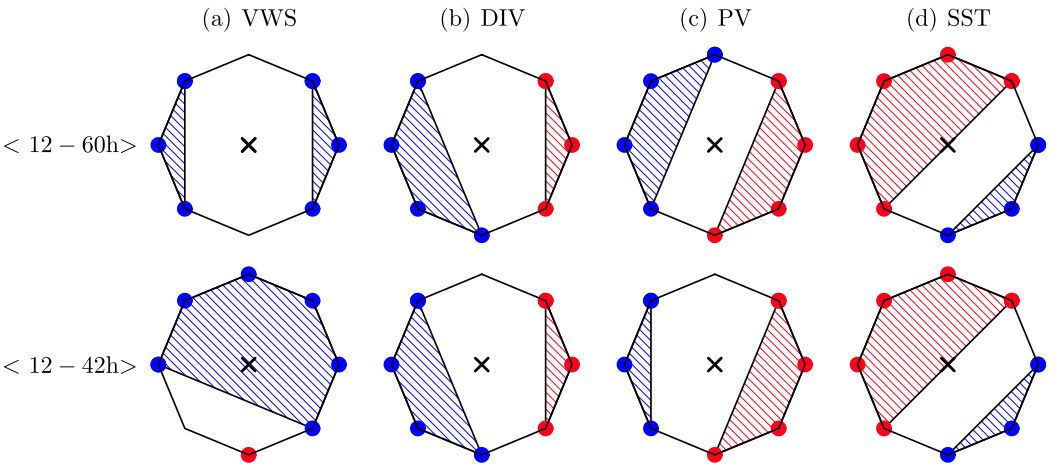

FIG. 8. Systematic favorable (red) and unfavorable (blue) octants for storm intensification for vortices initialized with the BT intensity at 1°, 2°, 3°, or 4° from the BT position. Octants are left blank if the parameter tendency varies with initial distances. The × indicates Dora's BT center at the initial time of the forecast and the solid circles indicate the octants in which the vortex is initially relocated. Four large-scale parameters are examined: (a) the 850–200-hPa wind shear (VWS), (b) the 200-hPa divergence (DIV), (c) the mean potential vorticity in the 335–350-K layer (PV), and (d) the SST. Parameters are averaged over the (first row) 12–60-h and (second row) 12–24-h period of the forecast and over a 200–800-km annulus surrounding the predicted storm center; except for the SST, which is averaged over a 200-km radius area.

correlation coefficient is highlighted in red. Note that, although PV advection was identified as a main mechanism for vortex intensification, we did not choose to use it directly as a predictor of TC intensification because it is a complex diagnostic that may not be suitable in an operational context. We use the mean 335–350-K PV instead.

Results are illustrated at t_0 + 36 h (Fig. 11), when the trough is at the closest distance from the TC (Fig. 6), which coincides with the first period of vortex intensification in the reference experiment (L13). The distributions of dots suggest an important spread of the forecasts with little or no relationship between the 850–200-hPa shear and either the central pressure or the divergence (Figs. 11b,e). Once again, in some cases the storm is more intense than in the reference experiment although the shear is larger (Fig. 11b, upper-left corner). For a few other experiments, a weaker shear is associated with higher central pressure (Fig. 11b, bottom-right corner). The relationship between the divergence and the shear is improved when using an ascending hierarchical classification to objectively split the ensemble into two groups or clusters (Fig. 11e). This method groups points that are the most similar and/or separates outliers that are far away from the main data. With six outliers removed (green dots), the main statistical relationship exhibits a decrease of divergence with shear ($r_1 = -0.5$, in blue). Conversely, the correlation between MSLP and VWS is not much improved when the sample is separated into two clusters (Fig. 11b).

In contrast, clear relationships with positive correlations exist at 36 h between DIV and −REFC (Fig. 11g), DIV and −PV (Fig. 11f), or PV and REFC (Fig. 11j). More than 50% and up to 81% of the variance is explained for those fits. Considering that the two metrics

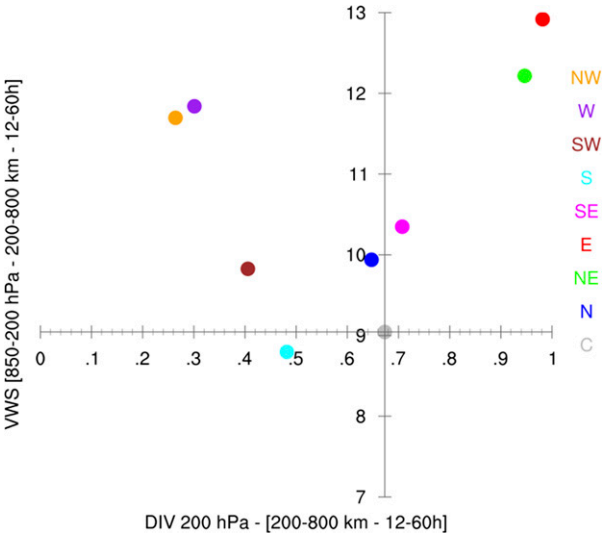

FIG. 9. The 850–200-hPa vertical wind shear (VWS, m s^{-1}) as a function of the 200-hPa divergence (10^{-5} s^{-1}) for experiments initialized with the BT intensity. Colors indicate the quadrant in which the initial vortex is displaced. Values are averaged for all initial distances (1° to 4°) over the 12–60-h period of the forecast and over a 200–800-km annulus surrounding the predicted storm center.

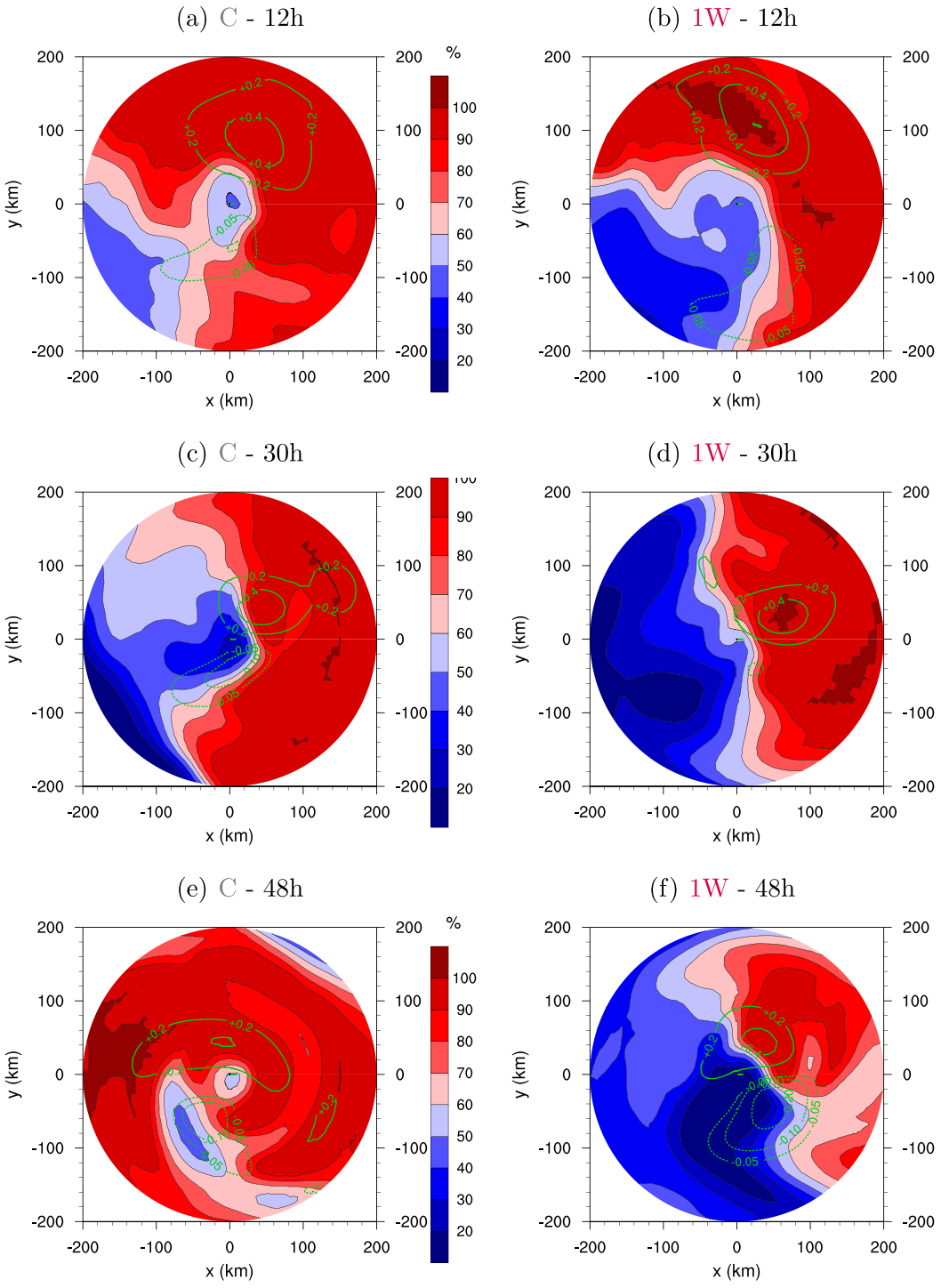

FIG. 10. The 500-hPa relative humidity (%) in a 200-km region around the TC center at different times of the simulation (left) for the reference experiment (C) and (right) for a BT-intensity vortex initially displaced 1° west (1W). Green dotted (solid) contours show negative (positive) 500-hPa vertical motion w ($\mathrm{m\,s^{-1}}$) approximated by $-\omega/10$. The vortex center is in the middle of the domain.

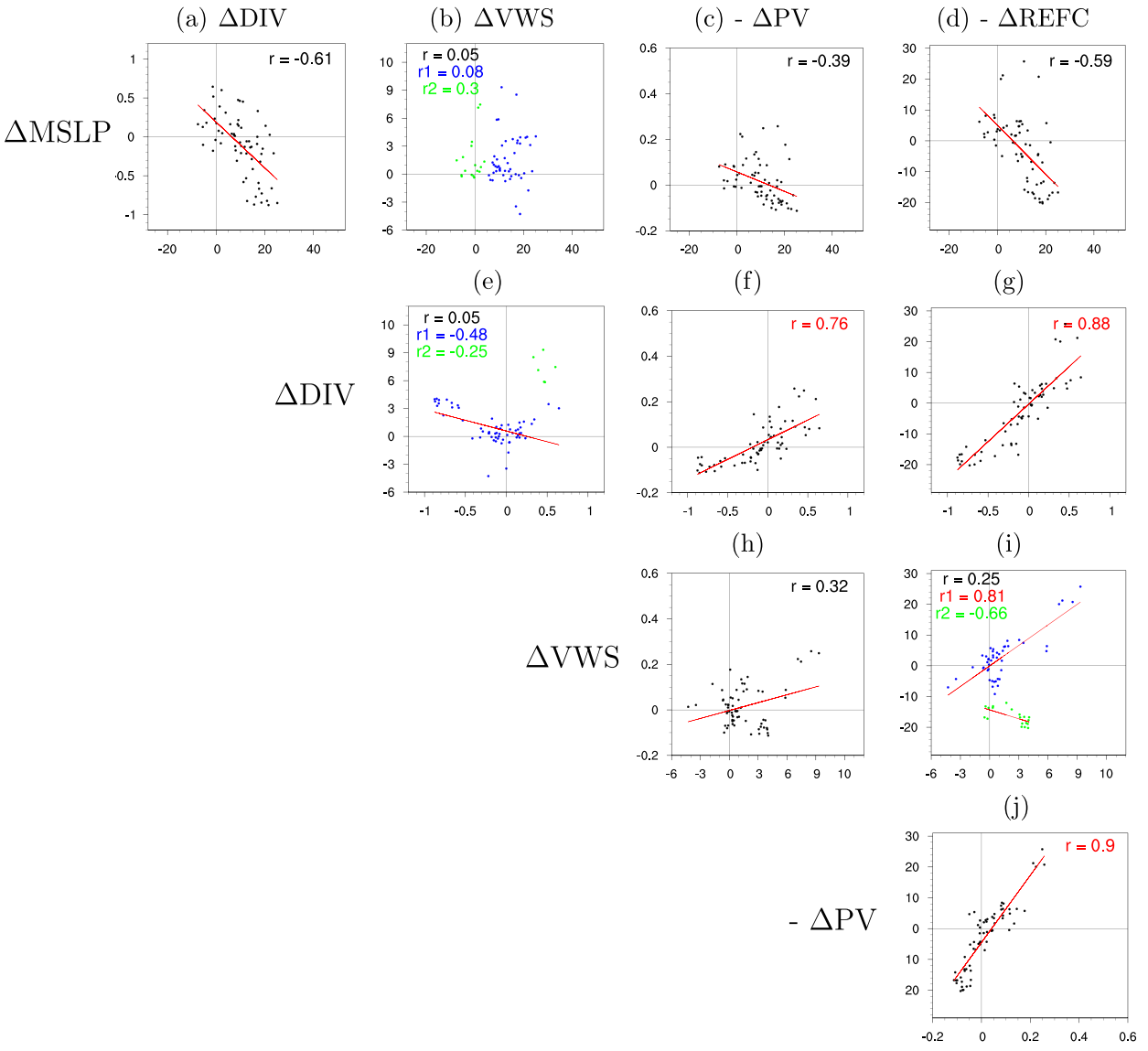

FIG. 11. Correlations between (from top to bottom) five analyzed variables with scatterplots of each variable (y in column) as a function of the other (x in row). Variables (VAR) are computed at t_0 + 36 h for 65 experiments (initialized at 975 and 960 hPa). The displayed values are differences with respect to the reference experiment (ΔVAR). MSLP (hPa) is the minimum sea level pressure change relative to the initial time (as in Fig. 5), DIV the 200-hPa divergence (10^{-5} s^{-1}), −REFC is the opposite value of the 200-hPa relative eddy flux convergence (m s^{-1} day^{-1}; positive for cyclonic angular momentum convergence), VWS the 850–200-hPa wind shear (m s^{-1}), and −PV the opposite value of the mean 335–350-K potential vorticity (PVU; positive for cyclonic values). DIV, VWS, PV, and REFC are averaged over the 200–800-km annulus range. The correlation coefficients of the standard linear regression between two variables (y in column; x in row) is given by r; red values indicate a high adjustment quality of the model ($r^2 \geq 50\%$). The best-fit line is drawn when r is statistically significant at the 95% level for $n - 2$ degrees of freedom; $n = 65$, except in (b), (e), and (i) where the data are split in two clusters of different sizes n_1 (blue) and n_2 (green) with coefficients r_1 and r_2 tested for $n_1 - 2$ and $n_2 - 2$ degrees of freedom.

REFC at 200 hPa and −PV in the 335–350-K layer both measure the import of cyclonic momentum, the fact that they are highly correlated is not surprising. There is also a statistically significant relationship at 36 h between MSLP and DIV (Fig. 11a), or MSLP and REFC (Fig. 11d), and to a minor extent between MSLP and PV (Fig. 11c), or shear and PV (Fig. 11h), although the explained variances are smaller. These results suggest, at least for this event, that when the trough is at the closest distance from the TC, (i) the 850–200-hPa shear is not a good predictor of TC intensification but the 200-hPa divergence, REFC, and PV are good predictors, and (ii) only one of the REFC, DIV, or PV parameter may be sufficient to diagnose or anticipate intensity changes, with

REFC or DIV showing higher correlation with the pressure change. Just like the shear, note nevertheless that for some cases storm intensification is weaker, while the divergence (or cyclonic REFC) is greater than the reference experiment. This indicates that the intensification process is not yet sufficiently well understood so that we can extract the governing parameters from available data.

At 42 h and beyond (not shown), the relationship between pressure and shear becomes significantly positive and peaks at 48 h, confirming the well-known fact that strong shear is detrimental to storm intensification. At 42 h, REFC and PV are still the best predictors for TC intensification but not afterward. When central pressure is considered at $t + 6$ h instead of t, the relationship between shear and pressure change is still statistically null at the 95% confidence level at 36 h, even though the correlation coefficient increases from 0.05 to 0.15. Meanwhile, the relationships between the pressure change and either DIV, −REFC, or −PV are still significant and only slightly weaker. When considering the pressure change at $t + 12$ h, the relationship with the shear at 36 h (and afterward) becomes statistically significant, with a marked increase in explained variance reaching 77% at 48 h. This suggests that storm intensification at 36–48 h may be closely tied to the shear value at and after 36 h in this set of experiments. It is also consistent with the delayed effect of shear on MSLP change documented in Frank and Ritchie (2001).

Smaller correlation coefficients are generally obtained when the REFC is averaged over different radial ranges such as 200–500 km, or 100–600 km as in Kaplan et al. (2010), or 300–600 km as in L13, DeMaria et al. (1993), or Hanley et al. (2001). The REFC computed over the 200–800-km region seems more helpful, at least for this event, to quantify a TC–trough interaction and its impact on TC intensity when the trough is initially located more than 1000 km away from the storm center.

5. Investigation of interesting simulations

This section attempts to highlight the major factors responsible for the intensification of vortices displaced 1° from the BT position in the eastern semicircle. Vortices moved farther away are also analyzed to identify possible alternative scenarios of TC–trough interaction.

a. Vortices close to the BT center

So far, a few explanations have been proposed to understand why the vortex displaced 1° northeast (1NE) does not intensify as much as the one displaced 1° southeast (1SE, Fig. 5). Compared to the reference experiment, the 1NE vortex benefits from slightly warmer seas over the 60-h period (a marginal mean +0.05°C),

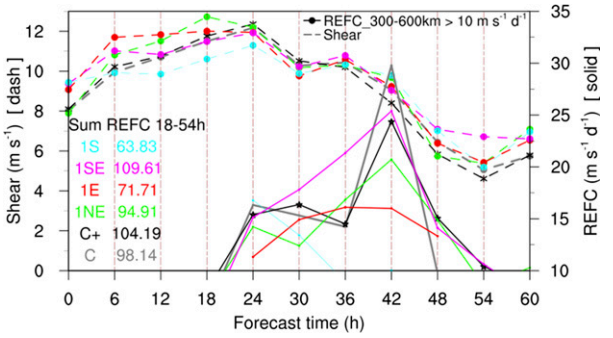

FIG. 12. Evolution of the predicted 850–200-hPa vertical wind shear ($m\,s^{-1}$, left axis, dashed lines) and relative eddy momentum flux convergence (REFC) modulus $>10\,m\,s^{-1}\,day^{-1}$ (right axis, solid lines) every 6 h from t_0 and for six experiments: the reference (C, gray), a stronger initial BT-position vortex (C+, black with asterisks), a BT-intensity vortex initially placed 1° northeast (green), east (red), southeast (magenta), and south (cyan). Inset notations at the bottom-left corner indicate REFC modulus values summed from 18 to 54 h.

stronger upper-level divergence ($+0.1\,10^{-5}\,s^{-1}$), slightly more cyclonic PV over a 200–800-km area and 335–350-K layer (−0.017 PVU), with, however, stronger wind shear during the first 24-h period and after 42 h, and slightly weaker accumulated REFC from 18 to 54 h (Fig. 12). On the contrary, compared to the reference experiment, the 1SE vortex has to face colder seas over the 60-h period (−0.1°C on average), a similar divergence, longer PV advection at 400 hPa (Figs. 6g–i), stronger mean large-scale PV (−0.04 PVU), much greater accumulated REFC from 18 to 54 h (albeit with a smaller maximum), and higher wind shear before 12 and after 42 h (Fig. 12). The PV advection associated with strong relative angular momentum flux convergence between 24 and 48 h, therefore, seems to be the prevailing factor for vortex deepening. Note that, while the 850–200-hPa wind shear surrounding the vortex displaced 1° south (1S) is reduced during the first 36-h period, the vortex has to face lower accumulated REFC (Fig. 12) and colder SST (−0.05°C on average over the 60-h period) than the vortex displaced 1° east (1E) and, consequently, it intensifies slightly less (Fig. 5). Also, at 400 hPa (as in Fig. 6), cyclonic PV advection from the trough into the 1S vortex does not last long (not shown).

A key aspect for TC intensification may, therefore, rely on how the merging between the trough and storm PV structures is effectively processed by the TC inner core. As can be seen in Fig. 6, PV anomalies associated with the trough and the TC have similar magnitudes around 400 hPa. The PV can be advected toward the TC core by the inward southeasterly flow associated with the trough at midlevels (the so-called inflow channel). But it can also be transported outward with the TC

upper-level divergent circulation (Figs. 6 and 7). Figure 7 further indicates that the PV radial advection penetrates deeper in the inner core of the 1SE vortex, and to a lesser extent in that of the 1NE vortex, than that of the reference experiment.

To quantify inner-core PV and its evolution, a PV budget is performed in a 300-km-radius cylinder vertically bounded by two isentropes at 305 and 350 K (details and equations can be found in L13). The total PV flux corresponds to the advective flux integrated over the cylinder's lateral surface. For a stronger initial vortex placed at the BT position, slightly more negative (cyclonic) PV anomalies are brought into the cylinder (NI curve) and significantly less negative PV anomalies are ejected from the cylinder (NO curve), resulting in larger cyclonic PV advection in the TC inner core (Fig. 13). This could explain the greater intensification rate of this vortex from 36 to 42 h compared to the reference experiment (Fig. 5, black stars). The two vortices initialized with the BT intensity, but displaced 1° southeast (1SE) or northeast (1NE), also benefit from stronger inward cyclonic PV fluxes. However, they have greater outward cyclonic PV fluxes with strong oscillations that impact the total cyclonic PV flux. The total PV flux in the 1SE vortex is slightly stronger after 36 h, in relation with the stronger rate of intensification observed after 36 h (Fig. 5, magenta circles). In contrast, PV fluxes in the inner core of the 1NE vortex become greater only after 46 h on average, consistent with Figs. 6j–l. The timing of vertically integrated cyclonic PV import from the trough is, therefore, critical to allow further storm intensification.

Examination of the equivalent potential temperature (θ_e) in the storm's inflow layer offers a complementary explanation for the intensification failure of the 1NE vortex after 36 h, compared to the reference experiment and to the 1SE vortex. The impact of dry air is investigated here by computing the downward flux of θ_e at the top of the boundary layer (850 hPa). Following Riemer et al. (2010), DFX $\equiv w_{\downarrow}\theta_e'$, where $w_{\downarrow}$ is negative vertical motion and the prime on θ denotes a deviation from the azimuthal mean. Parameters θ_e and $w_{\downarrow}$ are computed relative to the reference experiment. Positive values of DFX differences in Fig. 14 denote downward fluxes of cooler and drier (lower θ_e) air originating from above and penetrating into the boundary layer. Significant positive DFX values are found approximately in a semicircle around the 1NE storm center, just outside the radius of maximum winds, intruding radially inward toward the eyewall that is slowly contracting from about 40 km at 36 h to 30 km at 54 h. These persistent fluxes are associated with a large zone of dry air that gradually encircles the western then northern side of the storm at 500 hPa and above (as in Figs. 10b,d,f). They are also associated with shear-induced asymmetric downdrafts (Fig. 14) located underneath and downwind of the updrafts, in the downshear right (Southern Hemisphere) to upshear quadrant of the storm (Riemer et al. 2010). DFX differences are less pronounced for the 1SE vortex, in correlation with—and possibly because of—reduced downdrafts (Figs. 14b,d,f,h). Similarly, downward fluxes of θ_e for the reference experiment and for the stronger initial BT-position vortex are quite similar (not shown). Following Riemer et al. (2010), it is hypothesized that downward fluxes depress near-core θ_e values. Low θ_e air is then rapidly advected horizontally by the low-level radial inflow to the eyewall region, before latent and sensible heat fluxes from the ocean surface can restore large θ_e values. Reduced θ_e values within the eyewall updrafts of the 1NE vortex significantly impinge on the storm's energy cycle and intensification. The nonintensification of an initial weaker BT-position vortex is also associated with strong positive DFX fluxes in the inflow layer (not shown).

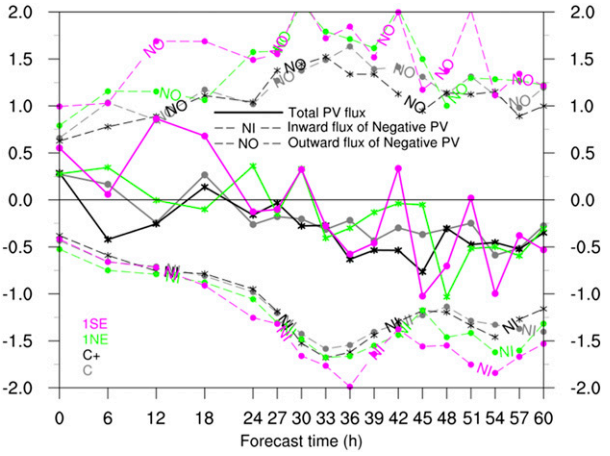

FIG. 13. Time evolution of the PV budget and two of its major components ($10^4\,m^5\,K\,s^{-2}\,kg^{-1}$) computed for a 300-km-radius cylinder centered on the TC and between 305 and 350 K for four experiments: the reference (C, gray circles), a stronger initial BT-position vortex (C+, black asterisks) reference experiment, at the top of the inflow layer, defined as 850 hPa, from $t_0 + 36$ to $t_0 + 54$ h, and for two experiments: a BT-intensity vortex initially displaced 1° northeast (1NE, green) or southeast (1SE, pink). Black dotted (solid) contours show negative (positive) 850-hPa vertical motion w ($m\,s^{-1}$) approximated by $-\omega/10$. The vortex center is in the middle of the domain.

b. *Vortices moved closer to the trough*

Also interesting is the fact that several sensitivity experiments that do not intensify much were able to reproduce a scenario very similar in space and time to the case of TC Fobane (2014) illustrated in Figs. 2b,d,f. Such a scenario occurs for vortices moved 3° or 4° east

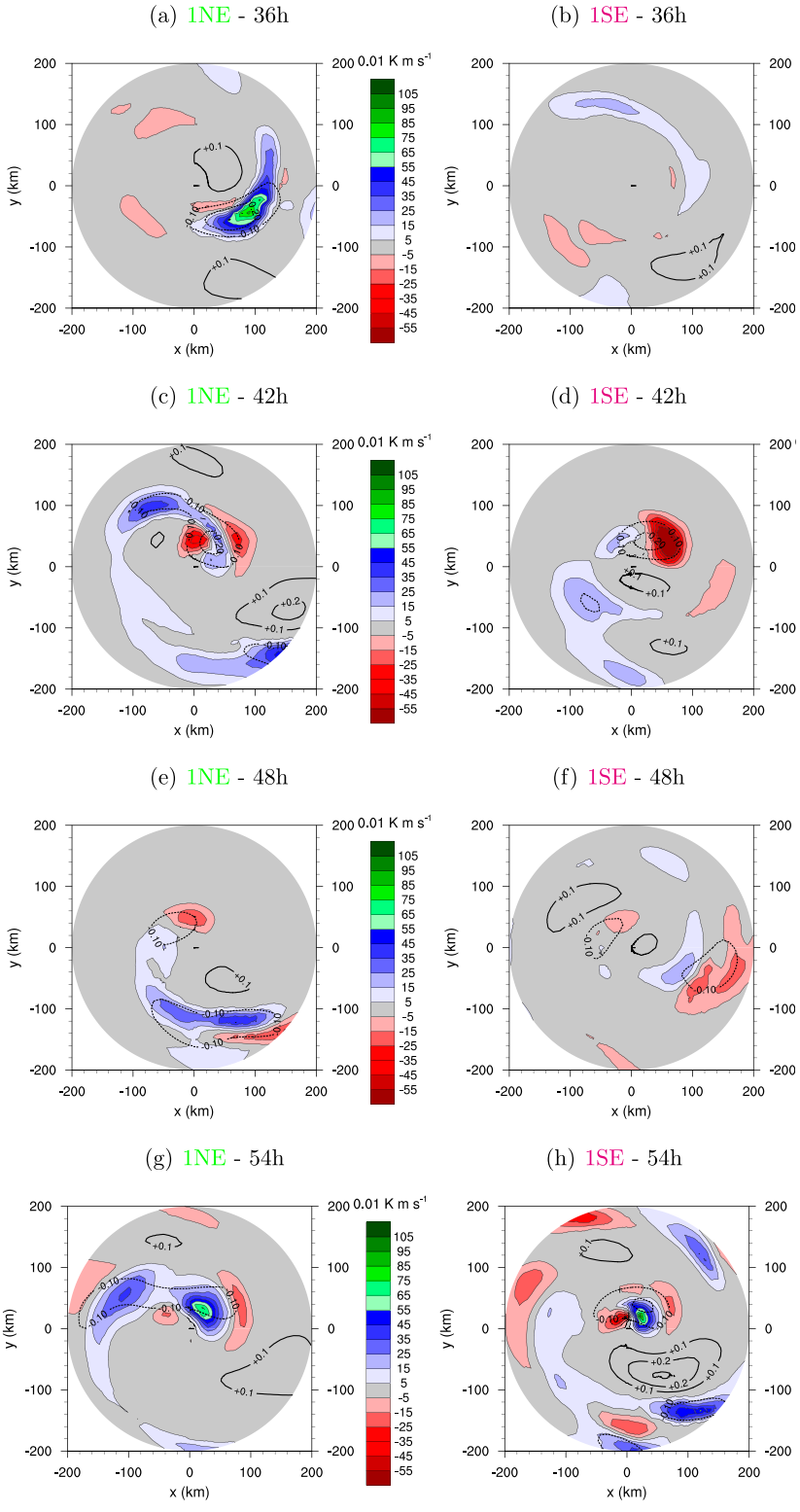

FIG. 14. Downward flux of θ'_e (color, in 0.01 K m s^{-1}) relative to the reference experiment, at the top of the inflow layer, defined as 850 hPa, from t_0 + 36 to t_0 + 54 h, and for two experiments: a BT-intensity vortex initially displaced (left) 1° northeast (1NE) or (right) 1° southeast (1SE). Black dotted (solid) contours show negative (positive) 850-hPa vertical motion w (m s^{-1}) approximated by $-\omega/10$. The vortex center is in the middle of the domain.

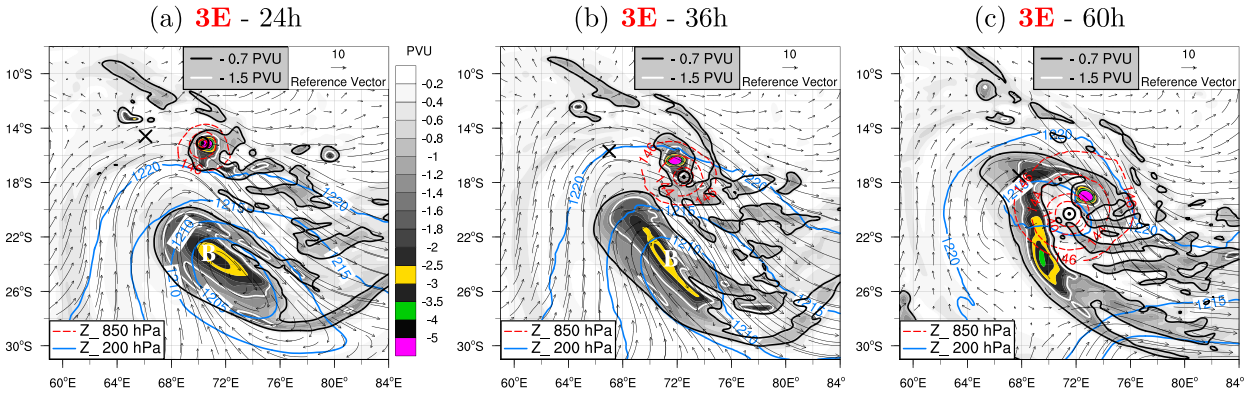

FIG. 15. As in Fig. 2, but at (a) t_0 + 24, (b) t_0 + 36, and (c) t_0 + 60 h into the model integration for the BT-intensity vortex initially displaced 3° east of the BT position. A black encircled dot (×) indicates the vortex predicted center in the simulation (in the reference experiment). Label B as in Figs. 3 and 6.

or northeast of the BT position. No matter their initial central pressure, the final intensity is 22 to 41 hPa higher than that of the reference vortex (Table 2). The PV evolution for the BT-intensity vortex displaced 3° east (3E) exemplifies this scenario (Fig. 15). At midlevels (330 K), potential vorticity from the trough is stretched by the storm's cyclonic flow. It wraps around, and eventually toward, the TC center in thin filaments until 60 h, as in Fig. 2f. Meanwhile, the 200-hPa cutoff low and the storm rapidly rotate cyclonically around each other in a manner similar to the Fujiwhara (1921) effect. The 200-hPa cutoff low remnant (blue contours) eventually moves on top of the TC low-level center (red contours) as in Fig. 2f. Considering the observed weakening of Fobane after t_2 + 42 h (Fig. 2d) and the simulated increase of central pressure after t_0 + 42 h in this set of sensitivity experiments, we can conclude that this scenario is clearly unfavorable for sustained TC intensification.

In fact, TC intensification in response to PV advection from a nearby trough may depend on the proximity of the main trough core. The trough approaching vortices in Figs. 6 and 7 gradually deforms and tilts toward the equator at midlevels, allowing cyclonic PV advection toward the TC core within a deep tropospheric layer above 335 K or 450 hPa. The initial anticyclonic and divergent circulation above Dora (Fig. 2a) favored the equatorward tilting of the trough and the formation of a spiral-like filament of PV ahead of the trough (Figs. 2c,e). Such a configuration with the main trough core (blue contours) and associated jet at a reasonable distance from the TC (Figs. 2c,e) increased upper-level divergence while preventing the most destructive part of the shear to affect the storm (L13). Once Dora's cyclonic circulation and associated convection strengthened, the induced outflow prevented further PV advection toward the center (cyclonic PV values spiraled at the outskirts of the TC core, Fig. 2e) and the trough went away rapidly.

For TC Fobane and the 3E, 3NE, 4E, or 4NE simulations, the interaction evolved in a different manner and resembled a merging event. A comparison of the fields at 330 and 350 K (not shown) indicates almost no tilting of the trough. The main trough core (PV anomaly and cyclonic flow) at mid- (Figs. 2d,f and 15) and upper (not illustrated) levels got close to the TC and almost moved on top of the cyclonic circulation. The positive effect of PV advection did not last long enough to temper the negative effect of the main trough core superposition. It remains unclear why the superposition of the main trough core on top of the TC cyclonic circulation is unfavorable for further intensification, but three hypotheses can be proposed. First, there is an imbalance between (i) the subsidence and radial convergence beneath the trough and (ii) the upward motion and induced outflow associated with the TC convection, so the TC suffocates. Second, when the trough and TC core are aligned (or moving in phase), there is a loss of REFC, a key ingredient for TC intensification as shown earlier. Third, when the two cyclonic circulations have equivalent scale and strength at midlevels, it allows direct advection or superposition of comparable PV values from the trough into the TC core. It is not the case at 350 K where PV values are much stronger in the trough than in the TC core and may unbalance the TC system.

These two contrasting scenarios (TC Fobane vs Dora) show how important for TC intensification is the establishment of an efficient inflow channel, through which PV values are transferred from the trough into the TC inner core at midlevels, while the main trough core stays at a reasonable distance not to impinge on the storm circulation.

6. Discussion and conclusions

The present study examines the sensitivity of TC intensification in the presence of a nearby upper-level trough and attempts to quantify forecast uncertainty. An ensemble of sensitivity experiments is generated from a realistic numerical simulation of a TC–trough interaction event using a hydrostatic limited-area model at 8-km resolution. While operational analyses of atmospheric and oceanic fields are not modified, the initial vortex is relocated to different positions with various strengths to account for the multiple plausible alternative scenarios observed in the tropics when a midlatitude trough approaches a TC. One-quarter of the initial perturbations are built within the current uncertainty in NWP analyses of both TC intensity and position. The previously investigated control run is used as a benchmark to assess the quantitative impact of upper-level forcing on TC track and intensity change.

In the control run and in the sensitivity experiments prone to intensification, the trough approaching the vortex gradually deforms and tilts toward the equator at midlevels. It allows cyclonic PV advection toward the TC core via an ''inflow channel'' located at midlevels (330–335 K, or about 500–450 hPa) after about 36 h, a mechanism responsible for the first rapid intensification period of Dora in the control run (L13). Such a configuration with the main upper-level trough core and associated jet at a reasonable distance from the TC increases upper-level divergence while preventing the strongest shear to affect the storm.

The relative positions of the interacting TC and upper-level low appear of major importance for TC intensification. Results show that in the Southern Hemisphere, the southern quadrant of a TC approached at a reasonable distance by an upper-level low, originally located to the southeast, benefits from favorable conditions in terms of upper-level divergence, vertical wind shear, and cyclonic potential vorticity. When the vortex is moved to the southwest, west, or northwest instead, the shear amplifies and the divergence decreases compared to the reference experiment, setting a relatively unfavorable environment for storm intensification. The tongue of dry air that gradually encircled the western side of TC Dora in association with the stratospheric air intrusion (L13) prevents vortices displaced toward the west to intensify more than the reference experiment. The vortex positions favorable for storm intensification are the ones that foster the development and maintenance of the inflow channel. When the vortex is displaced 3° or 4° east or northeast of the BT position, the 200-hPa cutoff low gets closer to the vortex and has a deleterious effect on its evolution. The cutoff low strongly influences the storm track (Fujiwhara effect) and induces a southward acceleration, allowing PV axisymmetrization around the TC core, but preventing intensification due to stronger shear and upper-level cyclonic flow superposition over the storm low-level cyclonic circulation. Such situations can explain cases of unfavorable TC–trough interaction observed in the southwest Indian Ocean (e.g., TC Fobane 2014), suggesting that the initial geometry of TC–trough interaction plays a major role in TC intensity changes.

The interaction promotes higher rates of intensification for vortices at initial tropical storm or TC stage (975 or 960 hPa). Initial tropical depressions (990 hPa) intensify considerably less, suggesting a sensitivity between the depth of the TC and the strength of the interaction. When the vortex is initially stronger (−10 hPa) and located at the best-track position, the rate of intensification is more dramatic (a relative −18 hPa in the course of 42 h) thanks to an extended inflow channel. Conversely, radial inflow and PV advection are delayed for a weaker initial vortex, and associated with a weaker rate of intensification.

A first conclusion is that the native geometry separating TC Dora from the upper-level low seemed ideal for positive interaction. However, had the storm been initially stronger or the trough 11° instead of 12° southeast of the vortex center, the TC could have been closer to its maximum potential intensity, which answers one of Kimball and Evans (2002)'s questions: whether the presence of a trough can get a TC closer to its potential intensity.

A statistical analysis of the 65 experiments show that the relationship between shear, divergence, and intensity change is not systematic. The 850–200-hPa shear is not a statistically good predictor for TC intensity change before 42-h of model integration for this case, when the trough moves away from the storm. The potential vorticity averaged over a thick 335–350-K layer and a 200–800-km annulus surrounding the predicted storm center appears to be a good indicator of trough proximity, at least for this event. Such a parameter could be used in climatological studies (following Kaplan and DeMaria 2003; Kaplan et al. 2010) to evaluate the relative impact of nearby troughs on the rapid intensification of tropical systems, in the southwest Indian Ocean and in other basins. Of course, the PV averaged over the limited sector of the trough rather than in a whole annulus might give a stronger trough signature. In the context of TC–trough interaction, the 200-hPa divergence and the 850–200-hPa shear do not necessarily evolve in the same way as usually believed. It may indeed be difficult to estimate the impact of asymmetric processes through symmetrically averaged quantities. This might be part of the difficulty to forecast good versus bad trough interactions in a systematic way.

It fosters the need to revisit our traditional limited-number-of-layers approach of the vertical wind shear and develop an interpretative measure (both in intensity and direction) of VWS in varying depth, or a diagnostic that would best reflect its total effect (both dynamic and thermodynamic) on TC intensity change.

Given the large forecast variability in the context of TC–trough interaction after 60 h of model integration and given that the geometry of the interaction controls both the future trough and TC structures and intensities, this study points to the importance of correctly initializing TC intensity and position, and not only large-scale upper-tropospheric structures. Needless to say, bogusing methods are not the panacea. They should soon be replaced by the possibility of assimilating cloud-affected microwave radiances (Bauer et al. 2010) and winds from scatterometers to constrain initial storm structure over data-sparse oceanic regions with no routine aircraft reconnaissance such as the southwest Indian Ocean.

Although based on one particular storm, this work gives some insight on the sensitivity of storm intensification to upper-level forcing in a real atmospheric and oceanic environment. It paves the route toward developing a TC–trough conceptual model for intensity purposes. The numerical methodology based here on real storm and trough interaction differs from previous highly idealized simulations in that the sensitivity to the TC strength and position was investigated here in place of the sensitivity to the trough size and structure. However, the main caveat is that it relies on vortex specification through bogusing so that the structure of the storm is imposed and the assimilation process tends to smooth out the forced initial values of TC intensity. To design a conceptual model, future studies could look at other radial ranges to compute both the VWS and the divergence since the relative distance seems important in such interactions. Other levels could also be used to compute diagnostic parameters such as the REFC, divergence, and shear, especially when the asymmetric radial circulation imposed by the trough affects a deep layer down to 500 hPa, as for TC Dora. As a large part of the inflow in the secondary circulation occurs above the boundary layer in such interactions, the modulation of the storm's secondary circulation would be worth investigating thoroughly. Fine details of the vortex's primary structure may also influence the response to shear, including intensity change. These studies would require the use of a (nonhydrostatic) numerical model at kilometer-scale resolution.

Acknowledgments. The authors would like to acknowledge the support of the mutuelle d'assurance des instituteurs de France (MAIF) foundation for cosponsoring this project. Thanks are extended to David Barbary for providing scripts to conduct statistics over the southwest Indian Ocean and to the development team (Rémy Lee-Ah-Siem) that continually works to improve model verifications. The authors are also indebted to Dr. Noel Davidson for providing valuable suggestions on an earlier version of the manuscript, and greatly appreciated the thorough and constructive comments from three anonymous reviewers.

REFERENCES

Aemisegger, F., 2009: Tropical cyclone forecast verification: Three approaches to the assessment of the ECMWF model. M.S. thesis, Department of Environmental Systems Science, Institute for Atmospheric and Climate Science, Eidgenssische Technische Hochschule Zürich, Zürich, Switzerland, 89 pp. [Available online at http://www.iac.ethz.ch/doc/publications/TC_MasterThesis.pdf.]

Bauer, P., A. J. Geer, P. Lopez, and D. Salmond, 2010: Direct 4D-Var assimilation of all-sky radiances. Part I: Implementation. *Quart. J. Roy. Meteor. Soc.*, **136**, 1868–1885, doi:10.1002/qj.659.

Bolton, D., 1980: The computation of equivalent potential temperature. *Mon. Wea. Rev.*, **108**, 1046–1053, doi:10.1175/1520-0493(1980)108<1046:TCOEPT>2.0.CO;2.

Bosart, L. F., W. E. Bracken, J. Molinari, C. S. Velden, and P. G. Black, 2000: Environmental influences on the rapid intensification of Hurricane Opal (1995) over the Gulf of Mexico. *Mon. Wea. Rev.*, **128**, 322–352, doi:10.1175/1520-0493(2000)128<0322:EIOTRI>2.0.CO;2.

Chan, J. C. L., Y. Duan, and L. K. Shay, 2001: Tropical cyclone intensity change from a simple ocean–atmosphere coupled model. *J. Atmos. Sci.*, **58**, 154–172, doi:10.1175/1520-0469(2001)058<0154:TCICFA>2.0.CO;2.

Cione, J., and E. W. Uhlhorn, 2003: Sea surface temperature variability in hurricanes: Implications with respect to intensity change. *Mon. Wea. Rev.*, **131**, 1783–1796, doi:10.1175//2562.1.

Davidson, N. E., C. M. Nguyen, and M. J. Reeder, 2008: Downstream development during the rapid intensification of Hurricanes Opal and Katrina: The distant trough interaction problem. *28th Conf. on Hurricanes and Tropical Meteorology*, Orlando, FL, Amer. Meteor. Soc., 9B.4. [Available online at https://ams.confex.com/ams/28Hurricanes/techprogram/paper_138060.htm.]

——, and Coauthors, 2014: ACCESS-TC: Vortex specification, 4DVAR initialization, verification, and structure diagnostics. *Mon. Wea. Rev.*, **142**, 1265–1289, doi:10.1175/MWR-D-13-00062.1.

DeMaria, M., and J. Kaplan, 1994: A Statistical Hurricane Intensity Prediction Scheme (SHIPS) for the Atlantic Basin. *Wea. Forecasting*, **9**, 209–220, doi:10.1175/1520-0434(1994)009<0209:ASHIPS>2.0.CO;2.

——, J.-J. Baik, and J. Kaplan, 1993: Upper-level eddy angular momentum fluxes and tropical cyclone intensity change. *J. Atmos. Sci.*, **50**, 1133–1147, doi:10.1175/1520-0469(1993)050<1133:ULEAMF>2.0.CO;2.

——, C. R. Sampson, J. A. Knaff, and K. D. Musgrave, 2014: Is tropical cyclone intensity guidance improving? *Bull. Amer. Meteor. Soc.*, **95**, 387–398, doi:10.1175/BAMS-D-12-00240.1.

Duvel, J. P., C. Basdevant, H. Bellenger, G. Reverdin, J. Vialard, and A. Vargas, 2009: The Aeroclipper: A new device to

explore convective systems and cyclones. *Bull. Amer. Meteor. Soc.*, **90**, 63–71, doi:10.1175/2008BAMS2500.1.

Dvorak, V., 1984: Tropical cyclone intensity analysis using satellite data. NOAA Tech. Rep. NESDIS 11, 47 pp.

Emanuel, K. A., 1991: The theory of hurricanes. *Annu. Rev. Fluid Mech.*, **23**, 179–196, doi:10.1146/annurev.fl.23.010191.001143.

Frank, W., and E. Ritchie, 2001: Effects of vertical wind shear on the intensity and structure of numerically simulated hurricanes. *Mon. Wea. Rev.*, **129**, 2249–2269, doi:10.1175/1520-0493(2001)129<2249:EOVWSO>2.0.CO;2.

Franklin, J. L., 2008: 2007 National Hurricane Center forecast verification report. NOAA Tech. Rep., 68 pp.

Fujiwhara, S., 1921: The natural tendency towards symmetry of motion and its application as a principle in meteorology. *Quart. J. Roy. Meteor. Soc.*, **47**, 287–292, doi:10.1002/qj.49704720010.

Ge, X., T. Li, and M. Peng, 2013: Effects of vertical shears and midlevel dry air on tropical cyclone developments. *J. Atmos. Sci.*, **70**, 3859–3875, doi:10.1175/JAS-D-13-066.1.

Gu, J. F., Z.-M. Tan, and X. Qiu, 2015: Effects of vertical wind shear on inner-core thermodynamics of an idealized simulated tropical cyclone. *J. Atmos. Sci.*, **72**, 511–530, doi:10.1175/JAS-D-14-0050.1.

Hanley, D., J. Molinari, and D. Keyser, 2001: A compositive study of the interactions between tropical cyclones and upper-tropospheric troughs. *Mon. Wea. Rev.*, **129**, 2570–2584, doi:10.1175/1520-0493(2001)129<2570:ACSOTI>2.0.CO;2.

Heming, J., and J. Goerss, 2010: Track and structure forecasts of tropical cyclones. *Global Perspectives on Tropical Cyclones*, J. C. L. Chan and J. D. Kepert, Eds., World Scientific, 287–323.

Hendricks, E. A., M. S. Peng, B. Fu, and T. Li, 2010: Quantifying environmental control on tropical cyclone intensity change. *Mon. Wea. Rev.*, **138**, 3243–3271, doi:10.1175/2010MWR3185.1.

Holland, G. J., 1980: An analytic model of the wind and pressure profiles in hurricanes. *Mon. Wea. Rev.*, **108**, 1212–1218, doi:10.1175/1520-0493(1980)108<1212:AAMOTW>2.0.CO;2.

——, 1997: The maximum potential intensity of tropical cyclones. *J. Atmos. Sci.*, **54**, 2519–2541, doi:10.1175/1520-0469(1997)054<2519:TMPIOT>2.0.CO;2.

Hoskins, B. J., M. E. McIntyre, and A. W. Robertson, 1985: On the use and significance of isentropic potential vorticity maps. *Quart. J. Roy. Meteor. Soc.*, **111**, 877–946, doi:10.1002/qj.49711147002.

Kaplan, J., and M. DeMaria, 2003: Large-scale characteristics of rapidly intensifying tropical cyclones in the North Atlantic basin. *Wea. Forecasting*, **18**, 1093–1108, doi:10.1175/1520-0434(2003)018<1093:LCORIT>2.0.CO;2.

——, ——, and J. A. Knaff, 2010: A revised tropical cyclone rapid intensification index for the Atlantic and eastern North Pacific basins. *Wea. Forecasting*, **25**, 220–241, doi:10.1175/2009WAF2222280.1.

Kimball, S. K., and J. L. Evans, 2002: Idealized numerical simulations of hurricane–trough interaction. *Mon. Wea. Rev.*, **130**, 2210–2227, doi:10.1175/1520-0493(2002)130<2210:INSOHT>2.0.CO;2.

Leroux, M.-D., M. Plu, D. Barbary, F. Roux, and P. Arbogast, 2013: Dynamical and physical processes leading to tropical cyclone intensification under upper-level trough forcing. *J. Atmos. Sci.*, **70**, 2547–2565, doi:10.1175/JAS-D-12-0293.1.

——, and Coauthors, 2014: Intensity change: External influences. Rapporteur Rep., Topic 2.5, *Eighth WMO Int. Workshop on Tropical Cyclones (IWTC-VIII)*, Publ. WMO, Topic 2.5, Jeju, Korea, WMO, 2.5.0–2.5.8. [Available online at http://www.wmo.int/pages/prog/arep/wwrp/new/documents/Topic2.5_IntensityChange_ExternalInfluences.pdf.]

Marquet, P., 2014: On the definition of a moist-air potential vorticity. *Quart. J. Roy. Meteor. Soc.*, **140**, 917–929, doi:10.1002/qj.2182.

Molinari, J., and D. Vollaro, 1989: External influences on hurricane intensity. Part I: Outflow layer eddy momentum fluxes. *J. Atmos. Sci.*, **46**, 1093–1105, doi:10.1175/1520-0469(1989)046<1093:EIOHIP>2.0.CO;2.

——, S. Skubis, and D. Vollaro, 1995: External influences on hurricane intensity. Part III: Potential vorticity structure. *J. Atmos. Sci.*, **52**, 3593–3606, doi:10.1175/1520-0469(1995)052<3593:EIOHIP>2.0.CO;2.

——, ——, ——, F. Alsheimer, and H. E. Willoughby, 1998: Potential vorticity analysis of tropical cyclone intensification. *J. Atmos. Sci.*, **55**, 2632–2644, doi:10.1175/1520-0469(1998)055<2632:PVAOTC>2.0.CO;2.

Montgomery, M. T., and R. J. Kallenbach, 1997: A theory of vortex Rossby waves and its application to spiral bands and intensity changes in hurricanes. *Quart. J. Roy. Meteor. Soc.*, **123**, 435–465, doi:10.1002/qj.49712353810.

——, M. E. Nicholls, T. A. Cram, and A. B. Saunders, 2006: A vortical hot tower route to tropical cyclogenesis. *J. Atmos. Sci.*, **63**, 355–386, doi:10.1175/JAS3604.1.

Montroty, R., F. Rabier, S. Westrelin, G. Faure, and N. Viltard, 2008: Impact of wind bogus and cloud- and rain-affected SSM/I data on tropical cyclone analyses and forecasts. *Quart. J. Roy. Meteor. Soc.*, **134**, 1673–1699, doi:10.1002/qj.308.

Nguyen, M. C., M. J. Reeder, N. E. Davidson, R. K. Smith, and M. T. Montgomery, 2011: Inner-core vacillation cycles during the intensification of Hurricane Katrina. *Quart. J. Roy. Meteor. Soc.*, **137**, 829–844, doi:10.1002/qj.823.

Nolan, D. S., Y. Moon, and D. P. Stern, 2007: Tropical cyclone intensification from asymmetric convection: Energetics and efficiency. *J. Atmos. Sci.*, **64**, 3377–3405, doi:10.1175/JAS3988.1.

Pantillon, F., J.-P. Chaboureau, and E. Richard, 2016: Vortex–vortex interaction between Hurricane Nadine (2012) and an Atlantic cut-off dropping the predictability over the Mediterranean. *Quart. J. Roy. Meteor. Soc.*, doi: 10.1002/qj.2635, in press.

Patla, J. E., D. Stevens, and G. M. Barnes, 2009: A conceptual model for the influence of TUTT cells on tropical cyclone motion in the northwest Pacific Ocean. *Wea. Forecasting*, **24**, 1215–1235, doi:10.1175/2009WAF2222181.1.

Pfeffer, R. L., and M. Challa, 1981: A numerical study of the role of eddy fluxes of momentum in the development of Atlantic hurricanes. *J. Atmos. Sci.*, **38**, 2393–2398, doi:10.1175/1520-0469(1981)038<2393:ANSOTR>2.0.CO;2.

Plu, M., P. Arbogast, and A. Joly, 2008: A wavelet representation of synoptic-scale coherent structures. *J. Atmos. Sci.*, **65**, 3116–3138, doi:10.1175/2008JAS2618.1.

Puri, K., and Coauthors, 2013: Operational implementation of the ACCESS numerical weather prediction systems. *Aust. Meteor. Oceanogr. J.*, **63**, 265–284.

Riemer, M., and S. C. Jones, 2014: Interaction of a tropical cyclone with a high-amplitude, midlatitude wave pattern: Waviness analysis, trough deformation and track bifurcation. *Quart. J. Roy. Meteor. Soc.*, **140**, 1362–1376, doi:10.1002/qj.2221.

——, M. T. Montgomery, and M. E. Nicholls, 2010: A new paradigm for intensity modification of tropical cyclones: Thermodynamic impact of vertical wind shear on the inflow layer. *Atmos. Chem. Phys.*, **10**, 3163–3188, doi:10.5194/acp-10-3163-2010.

——, ——, and ——, 2013: Further examination of the thermodynamic modification of the inflow layer of tropical cyclones

by vertical wind shear. *Atmos. Chem. Phys.*, **13**, 327–346, doi:10.5194/acp-13-327-2013.

Ritchie, E. A., and R. L. Elsberry, 2007: Simulations of the extratropical transition of tropical cyclones: Phasing between the upper-level trough and tropical systems. *Mon. Wea. Rev.*, **135**, 862–876, doi:10.1175/MWR3303.1.

Schubert, W. H., M. T. Montgomery, R. K. Taft, T. A. Guinn, S. R. Fulton, J. P. Kossin, and J. P. Edwards, 1999: Polygonal eyewalls, asymmetric eye contraction, and potential vorticity mixing in hurricanes. *J. Atmos. Sci.*, **56**, 1197–1223, doi:10.1175/1520-0469(1999)056<1197:PEAECA>2.0.CO;2.

Shapiro, L. J., and D. Möller, 2003: Influence of atmospheric asymmetries on the intensification of Hurricane Opal: Piecewise PV inversion diagnosis of a GFDL model forecast. *Mon. Wea. Rev.*, **131**, 1637–1649, doi:10.1175//2552.1.

——, and ——, 2005: Influence of atmospheric asymmetries on the intensification of GFDL model forecast hurricanes. *Mon. Wea. Rev.*, **133**, 2860–2875, doi:10.1175/MWR3008.1.

Shay, L. K., G. J. Goni, and P. G. Black, 2000: Effects of a warm oceanic feature on Hurricane Opal. *Mon. Wea. Rev.*, **128**, 1366–1383, doi:10.1175/1520-0493(2000)128<1366:EOAWOF>2.0.CO;2.

Shieh, O. H., M. Fiorino, M. E. Kucas, and B. Wang, 2013: Extreme rapid intensification of Typhoon Vicente (2012) in the South China Sea. *Wea. Forecasting*, **28**, 1578–1587, doi:10.1175/WAF-D-13-00076.1.

Shu, S., Y. Wang, and L. Bai, 2013: Insight into the role of lower-layer vertical wind shear in tropical cyclone intensification over the western North Pacific. *Acta Meteor. Sin.*, **27**, 356–363, doi:10.1007/s13351-013-0310-9.

——, F. Zhang, J. Ming, and Y. Wang, 2014: Environmental influences on the intensity changes of tropical cyclones over the western North Pacific. *Atmos. Chem. Phys.*, **14**, 6329–6342, doi:10.5194/acp-14-6329-2014.

Tang, B., and K. Emanuel, 2012: A ventilation index for tropical cyclones. *Bull. Amer. Meteor. Soc.*, **93**, 1901–1912, doi:10.1175/BAMS-D-11-00165.1.

Tao, D., and F. Zhang, 2014: Effect of environmental shear, sea-surface temperature, and ambient moisture on the formation and predictability of tropical cyclones: An ensemble-mean perspective. *J. Adv. Model. Earth Syst.*, **6**, 384–404, doi:10.1002/2014MS000314.

Vigh, J. L., and W. H. Schubert, 2009: Rapid development of the tropical cyclone warm core. *J. Atmos. Sci.*, **66**, 3335–3350, doi:10.1175/2009JAS3092.1.

Vincent, E. M., M. Lengaigne, G. Madec, J. Vialard, G. Samson, N. C. Jourdain, C. E. Menkes, and S. Jullien, 2012: Processes setting the characteristics of sea surface cooling induced by tropical cyclones. *J. Geophys. Res.*, **117**, C02020, doi:10.1029/2011JC007396.

Wang, Y., 2002: Vortex Rossby waves in a numerically simulated tropical cyclone. Part II: The role in tropical cyclone structure and intensity changes. *J. Atmos. Sci.*, **59**, 1239–1262, doi:10.1175/1520-0469(2002)059<1239:VRWIAN>2.0.CO;2.

——, Y. Rao, Z.-M. Tan, and D. Schönemann, 2015: A statistical analysis of the effects of vertical wind shear on tropical cyclone intensity change over the western North Pacific. *Mon. Wea. Rev.*, **143**, 3434–3453, doi:10.1175/MWR-D-15-0049.1.

Willoughby, H. E., J. A. Clos, and M. G. Shoreibah, 1982: Concentric eyewalls, secondary wind maxima, and the evolution of the hurricane vortex. *J. Atmos. Sci.*, **39**, 395–411, doi:10.1175/1520-0469(1982)039<0395:CEWSWM>2.0.CO;2.

WMO, 2007: *Sixth WMO International Workshop on Tropical Cyclones (IWTC-VI)*. Publ. WMO/TD-1383, WWRP 2007-1, San José, Costa Rica, World Meteorological Organization, 92 pp.

——, 2015: *Eighth International Workshop on Tropical Cyclones (IWTC-VIII)*. Publ. WMO, WWRP 2015-1, Jeju, Korea,World Meteorological Organization. [Available online at http://www.wmo.int/pages/prog/arep/wwrp/tmr/IWTC8.html.]

Yessad, K., 2015: Basics about ARPEGE/IFS, ALADIN and AROME in the cycle 42 of ARPEGE/IFS. Tech. reference manual, August 2015, Météo-France/CNRM/GMAP/ALGO, 64 pp. [Available at http://www.cnrm.meteo.fr/gmapdoc/spip.php?article29.]

Zeng, Z., Y. Wang, and L. Chen, 2010: A statistical analysis of vertical shear effect on tropical cyclone intensity change in the North Atlantic. *Geophys. Res. Lett.*, **37**, L02802, doi:10.1029/2009GL041788.

Zhang, D.-L., and H. Chen, 2012: Importance of the upper-level warm core in the rapid intensification of a tropical cyclone. *Geophys. Res. Lett.*, **39**, L02806, doi:10.1029/2011GL050578.

Zhang, F., and D. Tao, 2013: Effects of vertical wind shear on the predictability of tropical cyclones. *J. Atmos. Sci.*, **70**, 975–983, doi:10.1175/JAS-D-12-0133.1.